Available online at www.sciencedirect.com
SCIENCE DIRECT
Journal of Magnetic Resonance 180 (2006) 1–17
JMR Journal of Magnetic Resonance
www.elsevier.com/locate/jmr

Detection of correlated dynamics on multiple timescales by measurement of the differential relaxation of zero- and double-quantum coherences involving sidechain methyl groups in proteins

Armando Del Rio [a], Aditi Anand [a], Ranajeet Ghose [a,b,*]

[a] *Department of Chemistry, City College of the City University of New York, NY 10031, USA*
[b] *Graduate Center of the City University of New York, NY 10016, USA*

Received 15 October 2005; revised 2 January 2006
Available online 10 February 2006

Abstract

Multiple effects may lead to significant differences between the relaxation rates of zero-quantum coherences (ZQC) and double-quantum coherences (DQC) generated between a pair of nuclei in solution. These include the interference between the anisotropic chemical shifts of the two nuclei participating in formation of the ZQC or DQC, the individual dipolar interactions of each of the two nuclei with the same proton, and the slow modulation of the isotropic chemical shifts of the two nuclei due to conformational exchange. Motional events that occur on a timescale much faster than the rotational correlation time (ps–ns) influence the first two effects, while the third results from processes that occur on a far slower timescale (μs–ms). An analysis of the differential relaxation of ZQC and DQC is thus informative about dynamics on the fast as well as the slow timescales. We present here an experiment that probes the differential relaxation of ZQC and DQC involving methyl groups in protein sidechains as an extension to our recently proposed experiments for the protein backbone. We have applied the methodology to ^{15}N, ^{13}C-labeled ubiquitin and used a detailed analysis of the measured relaxation rates using a simple single-axis diffusion model to probe the motional restriction of the $C^{next}H^{next}$ bond vector where C^{next} is the carbon that is directly bonded to a sidechain methyl carbon (C^{methyl}). Comparison of the present results with the motional restriction of the $C^{next}C^{methyl}$ bond (S^2_{axis}) reveals that the single-axis diffusion model, while valid in the fringes of the protein and for shorter chain amino acids, proves inadequate in the central protein core for long chain, asymmetrically branched amino acids where more complex motional models are necessary, as is the inclusion of the possibility of correlation between multiple motional modes. In addition, the present measurements report on the modulation of isotropic chemical shifts due to motion on the μs–ms timescale. Three Leu residues (8, 50, and 56) are found to display these effects. These residues lie in regions where chemical shift modulation had been detected previously both in the backbone and sidechain regions of ubiquitin.

Keywords: Cross-correlated relaxation; Zero-quantum coherence; Double-quantum coherence; Methyl relaxation

1. Introduction

In the past few years, measurement of the interference or "cross-correlation" between two second rank tensorial interactions on the relaxation properties of various components of the density operator in scalar-coupled spin systems has provided a large amount of information inaccessible from conventional R_1, R_2 and steady-state NOE measurements [1,2]. These measurements have revealed the existence of anisotropic motion in the protein backbone [3] and have allowed the estimation of hitherto inaccessible backbone dihedral angles [4–7]. They have also provided the means to determine the chemical shift tensor for backbone amide ^{15}N [8–11], $^{13}C^{\alpha}$ [12], and carbonyl $^{13}C'$ [13,14] nuclei in solution.

Recent studies have shown that in addition to information on motion on the fast, ps–ns timescale,

* Corresponding author. Fax: +1 212 650 6107.
E-mail address: rghose@sci.ccny.cuny.edu (R. Ghose).

1090-7807/$ - see front matter © 2006 Published by Elsevier Inc.
doi:10.1016/j.jmr.2006.01.002

cross-correlated relaxation provides information on the slow, μs–ms timescale. Motion occurring on a timescale slower than the rotational correlation time, τ_c, which includes conformational exchange, manifests itself in a fashion similar to cross-correlated relaxation [15–17] in zero and double quantum coherences. These motions modulate "isotropic" spin-interactions like the scalar couplings [18] and isotropic chemical shifts [15,16] while the anisotropic interactions such as dipolar couplings and chemical shift anisotropy (CSA) are already motionally averaged by processes occurring on a timescale faster than τ_c. Unusually large differences in the relaxation rates between zero-quantum coherences (ZQC) and double-quantum coherences (DQC) generated between backbone amide ^{15}N and $^{1}H^{N}$ [16] nuclei and those between $^{13}C^{\alpha}$ and sidechain $^{13}C^{\beta}$ nuclei [17] were shown to be the result the cross-correlated modulation of the isotropic chemical shifts by exchange processes on the slow timescale. These effects were shown to be similar to those occurring as a result of cross-correlation between the CSAs of the two nuclei (vide infra) [16] that participate in the formation of the ZQC or DQC. However, the difference in timescales of the processes that modulate the two effects is evident from the fact that the effects of the cross-correlation between the isotropic chemical shifts modulated by slow dynamics can be refocused in a CPMG-type experiment [19,20]. Modulation of isotropic chemical shifts may occur due to a variety of reasons including variations in local dihedral angles, the formation or disruption of hydrogen bonds or rearrangement in the positioning of aromatic rings. These effects may be non-uniform for a set of nuclei and may provide information about correlated motion over multiple bonds [21], information that is inaccessible by conventional $R_{1\rho}$-type measurements [22].

Thus a careful analysis of the differential relaxation between ZQC and DQC has the potential to provide information about fast, local dynamics occurring on the ps–ns timescale as well as conformational exchange on the μs–ms timescale. So far, there has been some effort on measurement of the relaxation properties of ZQC and DQC in proteins. These studies have been focused on the protein backbone [16,21], on sidechain C^{α} and C^{β} nuclei [17,23] and on methyl groups [24,25]. There was a clear need to extend these studies to other sidechain positions in uniformly ^{13}C, ^{15}N-labeled proteins. We present here a new approach that measures the relaxation behavior of ZQC and DQC formed between a sidechain methyl ^{13}C (C^{methyl}) and the ^{13}C directly bonded to it (C^{next}) in uniformly ^{15}N, ^{13}C-labeled proteins. We further look at the feasibility of extracting information on the motional rigidity of the $C^{next}H^{next}$ bond (H^{next} is the proton that is directly bonded to C^{next}) through a detailed analysis of the rates and the inclusion of prior information about the motional rigidity of the $C^{next}C^{methyl}$ bond (S^2_{axis}) [26]. Since the $C^{next}C^{methyl}$ and $C^{next}H^{next}$ bonds are almost orthogonal, detection of differences in the motional rigidity of these two bonds should in principle provide clues into the presence of anisotropic motion in protein sidechains as indicated by Yang et al. [27] and analogous to those seen in the backbone regions of proteins [3]. In addition, the detection of very large differences between the ZQC and DQC relaxation rates that cannot be explained by fast, ps–ns dynamics alone are interpreted as the result of slow, correlated modulation of isotropic chemical shifts on the μs–ms timescale.

2. Theory

The imaginary part of the ZQ (ρ_{ZQ}) and DQ (ρ_{DQ}) components of the density operator (also referred to as the y-component or ZQ_y or DQ_y terms) in a scalar-coupled IS system may be expressed in the following way:

$$\rho_{ZQ} = \frac{1}{2}[2I_yS_x - 2I_xS_y] = \frac{1}{2i}[I_+S_- - I_-S_+], \tag{1a}$$

$$\rho_{DQ} = \frac{1}{2}[2I_yS_x + 2I_xS_y] = \frac{1}{2i}[I_+S_+ - I_-S_-], \tag{1b}$$

where ρ_{DQ} contains the ± 2 quantum terms. The evolution of ρ_{ZQ} and ρ_{DQ} over a period τ_M (neglecting chemical shift evolution and including only relevant terms of the density operator, i.e., those terms that lead to observable signal at the end of the experiment) is given by:

$$\rho_{ZQ}(\tau_M) = \prod_{l=1}^{m} \cos(\pi J^l_{ZQ}\tau_M)e^{-\Gamma_{ZQ}\tau_M}\rho_{ZQ}(0) + \cdots, \tag{2a}$$

$$\rho_{DQ}(\tau_M) = \prod_{l=1}^{m} \cos(\pi J^l_{DQ}\tau_M)e^{-\Gamma_{DQ}\tau_M}\rho_{DQ}(0) + \cdots \tag{2b}$$

$\Gamma_{ZQ}(\Gamma_{DQ})$ is the relaxation rate of the ZQ (DQ) term and the corresponding effective scalar coupling constant with the lth passive nucleus (X^l) is represented by $J^l_{ZQ}(J^l_{DQ})$. We have assumed that the I and S nuclei are coupled with m passive spins and J^l_{ZQ} and J^l_{DQ} are given by

$$J^l_{ZQ,DQ} = {}^aJ(I,X^l) \mp {}^bJ(S,X^l), \tag{3}$$

where the "−" sign holds for the ZQC and the "+" sign for DQC. The ${}^aJ(I,X^l)$ and ${}^bJ(S,X^l)$ represent the a/b-bond scalar couplings ($a,b = 1,2,3$) with a passive nucleus X^l. In the case where the $J^l_{ZQ,DQ}$ are dominated by large one-bond passive couplings with the I nucleus ($a = 1$, $b = 2$), Eq. (2) can to an excellent approximation, be written as (as in Eq. (2), only relevant terms are shown):

$$\rho_{ZQ}(\tau_M) = \cos(\pi J_{ZQ}\tau_M)^m e^{-\Gamma_{ZQ}\tau_M}\rho_{ZQ}(0) + \cdots, \tag{4a}$$

$$\rho_{DQ}(\tau_M) = \cos(\pi J_{DQ}\tau_M)^m e^{-\Gamma_{DQ}\tau_M}\rho_{DQ}(0) + \cdots, \tag{4b}$$

where $J_{ZQ,DQ} = {}^1J(I,X^l) \mp {}^2J(S,X^l)$. The difference between J_{DQ} and J_{ZQ} for a particular spin pair depends on multiple sidechain dihedral angles. However, in general, this dependence is rather complicated and the relationship with respect to a particular dihedral angle is difficult to determine for most amino-acid types using a simple analysis of $J_{ZQ,DQ}$ values (to analyze this accurately, one has to also take into account the small 2 and 3 bond couplings, i.e., consider Eqs. (2) and (3) instead of Eq. (4)).

In the general case, $\Gamma_{ZQ} \neq \Gamma_{DQ}$ and the difference ($\Delta\Gamma$) is given by (neglecting the contributions of the non-zero frequencies of the spectral density function, i.e., considering only $J(0)$ terms)

$$\begin{aligned}\Delta\Gamma &= \Gamma_{DQ} - \Gamma_{ZQ} \\ &= \frac{8}{9}B_0^2\left(\frac{2}{5}\tau_c\right)\sum_{i,j=1,2}\left(\sigma_{ii}^I - \sigma_{33}^I\right)\left(\sigma_{jj}^S - \sigma_{33}^S\right)P_2(\cos\theta_{ij})S_{ij}^2 \\ &\quad + 2\left(\frac{2}{5}\tau_c\right)\sum_k\left(\frac{\mu_0\hbar}{4\pi}\right)^2\frac{\gamma_H^2\gamma_I\gamma_S}{r_{IH^k}^3 r_{SH^k}^3}S_{k,\text{cross}}^2 \\ &\quad + \frac{1}{5}\left(\frac{2}{5}\tau_c\right)\left(\frac{\mu_0\hbar}{4\pi}\right)^2\frac{\gamma_I^2\gamma_S^2}{r_{IS}^6}S_{IS}^2 + 4\Delta\omega_I\Delta\omega_S p_A p_B\tau_{ex} \\ &= \sum_{i,j}R_{ij}^{CC} + \sum_k R_k^{DD} + R^{XR} + R^{ex}. \end{aligned} \quad (5)$$

The first term in Eq. (5) ($\sum_{i,j}R_{ij}^{CC}$) results from the cross-correlation between the fully asymmetric CSA tensors of the two spins I and S. The $\sigma_{jj}^{I,S}(\sigma_{11} \leqslant \sigma_{22} \leqslant \sigma_{33})$ represent the principal components of the two CSA tensors and the angle θ_{ij} denotes the projection of the ith component of the CSA tensor of spin I on the jth component of the CSA tensor of spin S; S_{ij}^2 is the Lipari–Szabo order-parameter for the interaction. The second term ($\sum_k R_k^{DD}$) in Eq. (5) results from the cross-correlation between the dipolar interactions of each spin I and S with the same proton H^k at a distance r_{IH^k} from spin I and r_{SH^k} from spin S, $S_{k,\text{cross}}^2$ is the cross-correlation order parameter (vide infra) for the interaction. The third term (R^{XR}) is due to the cross-relaxation between I and S (S_{IS}^2 is the order parameter describing the motional restriction of the IS internuclear vector and assuming that spins I and S constitute a homonuclear spin system in the Goldman [28] formalism, i.e., $\omega_I \approx \omega_S$; r_{IS} is the IS bond length). Dipole–dipole cross-correlations involving heteronuclear spins only are sufficiently small to be neglected in the present analysis. τ_c is the global rotational correlation time (assuming an isotropic rotational diffusion tensor) and $P_2(\cos\theta) = \frac{1}{2}(3\cos^2\theta - 1)$. All other terms have their usual meaning. The first three terms of Eq. (5) are modulated by the rotational reorientation and represent relaxation in the traditional Redfield sense. However, the fourth term (R^{ex}) appears as a result of two-state exchange with a time constant $1/\tau_{ex}$ between specific conformational states A and B with relative populations p_A and $p_B = 1 - p_A$, respectively. The difference in resonance frequencies between the two conformational states for spins I and S are $\Delta\omega_I$ and $\Delta\omega_S$, respectively [16]. Eq. (5) has been derived using a second-order perturbation approach (like Redfield theory) and is valid for $\tau_c \ll \tau_{ex} \ll \tau_\sigma$, where $\tau_\sigma = \frac{1}{\sqrt{\Delta\omega_I\Delta\omega_S}}$ characterizes an effective frequency (chemical shift) scale. In practice, this puts τ_{ex} in the μs–ms regime [21]. On this timescale (corresponding to fast exchange on the multiple quantum frequency scale) the linear dependence on τ_{ex} may result in very large differences between the relaxation rates of ZQC and DQC in the presence of conformational exchange. Further, it is implicitly assumed that the τ_M period (in Eq. (4)) is long compared to the exchange time τ_{ex}, i.e., $\tau_{ex} \ll \tau_M$ for all τ_M values, otherwise the apparent R^{ex} value estimated from $\Delta\Gamma$ using Eqs. (4) and (5) would have an explicit τ_M dependence. This is not expected to be an issue in the present study. In ubiquitin, τ_{ex} values have been found to vary between 0.2 and 0.4 ms [29]. These measurements though made from backbone experiments, are nevertheless expected to be valid in the present context since slow motions tend to be less local and sidechain τ_{ex} values are not expected to be significantly different.

Thus in order to measure $J_{ZQ,DQ}$ and $\Gamma_{ZQ,DQ}$ two sets of experiments are required—one set that measures the evolution of the ZQC and a second that measures the time-evolution of the DQC. The signal intensities in the two experiments as a function of a relaxation delay τ_M (assuming $\tau_{ex} \ll \tau_M$ for all τ_M values) are given by:

$$S_{ZQ}(\tau_M) = A_{ZQ}\cos(\pi J_{ZQ}\tau_M)^m e^{-\Gamma_{ZQ}\tau_M}, \quad (6a)$$

$$S_{DQ}(\tau_M) = A_{DQ}\cos(\pi J_{DQ}\tau_M)^m e^{-\Gamma_{DQ}\tau_M}, \quad (6b)$$

where A_{ZQ} and A_{DQ} are constants. Note, in writing Eqs. (5) and (6) we have assumed that the ZQC and DQC decays may be represented by single exponential functions, i.e., the secular approximation is valid. The validity of the secular approximation has been discussed in detail in the appendix (Appendix A).

3. Materials and methods

3.1. Experimental design

The pulse sequences utilized to measure the relaxation rates of ZQC and DQC involving a methyl sidechain ^{13}C nucleus ($^{13}C^{methyl}$) and the ^{13}C nucleus immediately preceding it ($^{13}C^{next}$) in uniformly ^{15}N, ^{13}C-labeled proteins are depicted in Fig. 1. The sequences are based on selective HSQC-type experiments common in the literature, so only the salient features are described. Coherences evolving as ZQ or DQ during τ_M were selected by simultaneously cycling the phases ϕ_2 and ϕ_3 [17]. ^{13}C–^{13}C scalar couplings are active during τ_M since the selective 180° pulse (indicated by the filled gray sine-bell in Fig. 1) applied at the center of the τ_M period inverts the entire aliphatic region. Use of pulsed field gradients for coherence selection instead of the elaborate phase-cycle utilized here is also plausible. However, in that case, simultaneous selection of both the +2 and −2 quantum coherences would not be possible, leading to a twofold decrease in signal intensity in the DQ-type experiment. An additional 16-step phase cycling (on ϕ_3 and ϕ_{rec}) was used in the sequence to detect the ZQC. This was required to eliminate two-spin order ($2I_zS_z$) that has similar transformation properties as the ZQC. These spurious terms may be generated by inaccuracies in pulses and delays prior to the relaxation period τ_M.

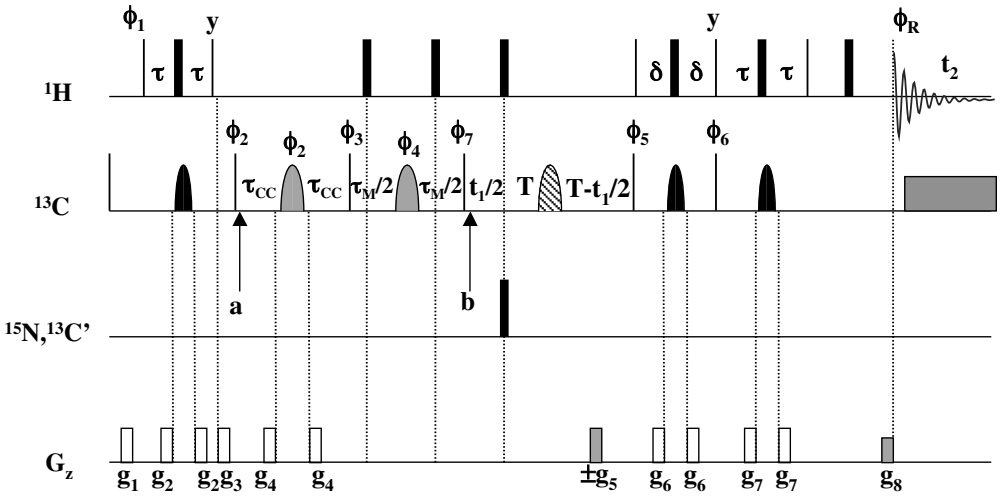

Fig. 1. Pulse sequences used to measure the decay rates of DQC (Γ_{DQ}) and ZQC (Γ_{ZQ}). 90° and 180° pulses are represented by narrow and thick lines, respectively. Shaped pulses are shown as sine-bells. The dark solid sine-bells represent methyl-selective 1.2 ms IBURP2 [46] pulses centered at 20 ppm, the light solid sine-bells represent 400 μs REBURP [46] pulses centered at 35 ppm and the hatched sine-bell represents an off-resonance 400 μs REBURP pulse centered at 35 ppm. The $^{1}H/^{13}C$ carriers are initially set at 1.0 ppm/20 ppm moved to 2.5 ppm/35 ppm at point 'a' and moved back to 1.0 ppm/20 ppm at point 'b.' The delays $\tau = 1/4J_{CH} = 1.9$ ms, $\tau_{CC} = 1/4J_{CC} = 7.1$ ms, and $T = 7.0$ ms. The following phase cycling is used $\phi_1 = \{x,-x\}$, $\phi_2 = \{4(x),4(y),4(-x),4(-y)\}$, $\phi_4 = \{x,y,-x,-y\}$, $\phi_5 = \{x,x,-x,-x\}$, $\phi_6 = \{y,y,-y,-y\}$ and $\phi_7 = \{x\}$. For the DQ datasets $\phi_3 = \{4(x),4(y),4(-x),4(-y)\}$ and $\phi_{rec} = \{x,-x,-x,x,-x,x,x,-x,x,-x,-x,x,x,-x,x,-x\}$. For the ZQ datasets $\phi_3 = \{4(x),4(y),4(-x),4(-y),4(-x),4(-y),4(x),4(y)\}$ and $\phi_{rec} = \{4(x,-x,-x,x),4(-x,x,x-x)\}$. All other pulses are applied along the $+x$ direction. The gradients g_1 (1 ms, 5 G/cm), g_2 (450 μs, 10 G/cm), g_3 (1.5 ms/13 G/cm), g_4 (800 μs, 10 G/cm), g_5 (1 ms, 13 G/cm), g_6 (450 μs, 2 G/cm), g_7 (500 μs, 11 G/cm), and g_8 (250 μs, 13 G/cm). The sign of the gradient pulse g_5 is inverted on alternate FIDs to obtain hypercomplex data. Decoupling was achieved during acquisition using a GARP sequence with a 2.9 kHz field.

The carrier was initially placed at 1.0 ppm for the ^{1}H channel and 20 ppm for the ^{13}C channel, i.e., at the center of the methyl region and shifted to 2.5 ppm (^{1}H) and 35.0 ppm (^{13}C) for efficient excitation of the entire aliphatic region at point 'a.' The carrier was shifted back to the methyl region at point 'b' for constant-time evolution of ^{13}C single quantum coherence and subsequent back transfer and detection utilizing the back-end of a gradient selected, sensitivity-enhanced HSQC [30]. Eq. (4) gives the time-evolution of the relevant components of the density operator during τ_M.

To be formally accurate, the relevant components of the density operator at the start and end of the τ_M period are given by $\rho_{ZQ_z} \propto [I_+S_- - I_-S_+]H_z$ or $\rho_{DQ_z} \propto [I_+S_- - I_-S_+]H_z$ in the ZQ-type or DQ-type experiments respectively. During τ_M, an oscillation takes place between ρ_{ZQ_z} and ρ_{ZQ} (given by Eq. (1a)) in the ZQ experiment and a corresponding oscillation between ρ_{DQ_z} and ρ_{DQ} (Eq. (1b)) occurs in the DQ experiment. Thus, the actual relaxation rates measured are the time-averaged [31] relaxation rates for ρ_{ZQ_z} and ρ_{ZQ} in the case of Γ_{ZQ} and ρ_{DQ_z} and ρ_{DQ} for Γ_{DQ}. This averaging may be incomplete for shorter τ_M values and more elaborate expressions that take this behavior into account in similar cases have been suggested [31]. Simulations show that in the present case, the errors in $\Gamma_{ZQ,DQ}$ resulting from the use of Eq. (6) as opposed to more exact expressions are far smaller than the experimental precision.

3.2. Data processing and analysis

All experiments were performed on a Varian Inova NMR spectrometer operating at 600 MHz and equipped with a triple-resonance HCN probe capable of applying pulsed field gradients along the z-axis. The total number of transients per t_1 point was 64 and a recycle delay of 1.5 s was used in all cases. The values of τ_M used were 0.5(×2), 4.0, 7.0, 14.3, 16.0, 22.0, 28.0(×2), 38.0, 42.9, 44.0, 50.0(×2), 58.0 and 71.5 ms. All experiments were performed at 30 °C on a 1.0 mM sample of ^{15}N, ^{13}C labled human ubiquitin in 50 mM sodium acetate, 90% H_2O, 10% D_2O and 0.1% NaN_3, pH 5.0. The sample conditions were consistent with those used previously [26] to justify the use of the S^2_{axis} obtained in that study in the present analysis. The data were processed using the NMRPIPE [32] suite of software. Mirroring was used in the indirect dimension followed by apodization using a squared cosine-bell function and zero-filling to double the data size prior to Fourier transformation. The data in the direct dimension were also apodized using a squared cosine-bell and zero-filled to double the size prior to Fourier transformation. The data from the ZQ and DQ datasets were fit to Eq. (6) using in-house software that utilized the ODRPACK [33] library. In the initial analysis, data points for all 17 τ_M values were fit to Eq. (6) to obtain accurate values of $J_{ZQ,DQ}$ which are essentially determined by the zeroes of Eq. (6). In the present case the $J_{ZQ,DQ}$ were dominated by the one-bond $^{1}J_{CC}$ couplings (C^{next} and its m directly bonded ^{13}C, $m = 0,1,2$). The values of m depend on the amino-acid type and the relevant coherences were grouped into three distinct classes (I, II, and III) as shown in Table 1. In the final analysis, the $J_{ZQ,DQ}$ determined from the initial analysis were held fixed and data for the first 10 τ_M values

Table 1
Classes of DQ/ZQ resonances based on number of one-bond passive couplings—see Eqs. (4) and (6)

Class	m	Residue type	I spin	S spin	Dominant $^1J_{CC}$
I	0	Ala	$^{13}C^{\alpha}$	$^{13}C^{\beta}$	None
II	1	Thr	$^{13}C^{\beta}$	$^{13}C^{\gamma}$	$^{13}C^{\alpha}$–$^{13}C^{\beta}$
II	1	Ile	$^{13}C^{\gamma 1}$	$^{13}C^{\delta 1}$	$^{13}C^{\beta}$–$^{13}C^{\gamma 1}$
III	2	Ile	$^{13}C^{\beta}$	$^{13}C^{\gamma 2}$	$^{13}C^{\alpha}$–$^{13}C^{\beta}$,$^{13}C^{\gamma 1}$–$^{13}C^{\beta}$
III	2	Leu	$^{13}C^{\gamma}$	$^{13}C^{\delta 1}$	$^{13}C^{\beta}$–$^{13}C^{\gamma}$,$^{13}C^{\delta 2}$–$^{13}C^{\gamma}$
III	2	Leu	$^{13}C^{\gamma}$	$^{13}C^{\delta 2}$	$^{13}C^{\beta}$–$^{13}C^{\gamma}$,$^{13}C^{\delta 1}$–$^{13}C^{\gamma}$
III	2	Val	$^{13}C^{\beta}$	$^{13}C^{\gamma 1}$	$^{13}C^{\alpha}$–$^{13}C^{\beta}$,$^{13}C^{\gamma 2}$–$^{13}C^{\beta}$
III	2	Val	$^{13}C^{\beta}$	$^{13}C^{\gamma 2}$	$^{13}C^{\alpha}$–$^{13}C^{\beta}$,$^{13}C^{\gamma 1}$–$^{13}C^{\beta}$

(upto and including $\tau_M = 28$ ms) were fit to Eq. (6) to obtain the $\Gamma_{ZQ,DQ}$. This two-step procedure is necessary, in general, to prevent any multi-exponential behavior in the ZQ/DQ decay at longer τ_M (Appendix A) values from affecting the rates [17] (The rates determined in ubiquitin remained the same within error even if the entire curve including all τ_M values was used, implying that non-secular effects may not be that important in small proteins in the present context. We however, chose to employ the two-step procedure for generality and consistency with previous work [17].) This two-step procedure was not necessary for Ala residues for which $m = 0$ in Eq. (6) and only the first 10 data points were used to obtain $\Gamma_{ZQ,DQ}$. Note that for coherences for which $m = 2$ in Eq. (6), an exact approach would require the use of different coupling constants for each of the passive couplings, i.e., $\cos(\pi J_{1,ZQ/1,DQ}\tau_M)\cos(\pi J_{2,ZQ/2,DQ}\tau_M)$ as opposed to $\cos(\pi J_{ZQ/DQ}\tau_M)^2$ in the argument. However, the use of an additional fitted parameter was not found to result in a statistically significant improvement in the quality of the fits for these coherences. As was mentioned previously, an additional 16-step phase cycle was introduced into the experiment to measure the time-evolution of ZQC in order to prevent the contamination by two-spin order terms (in reality these are three spin order terms of type $4H_zI_zS_z$) which have the same transformation properties as the ZQC and result from non-ideal behavior during the pulse sequence. This procedure however was unable to completely eliminate the contamination. We found that the quality of the fits for the ZQ datasets improved in a statistically significant way on including a τ_M independent offset in Eq. (6). The rates, Γ_{ZQ},

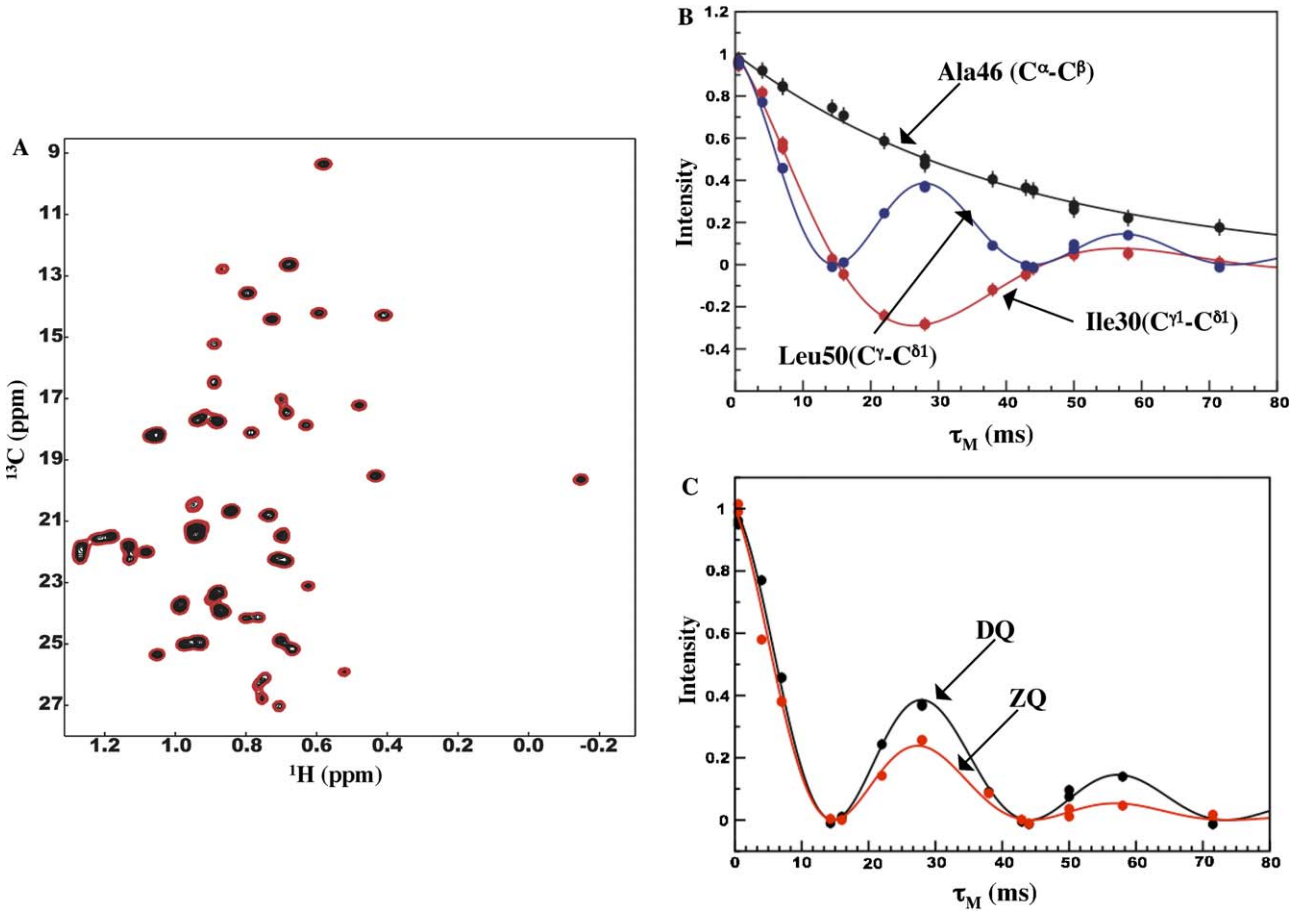

Fig. 2. (A) Representative double-quantum (red) and zero-quantum (black) datasets for ^{13}C, ^{15}N-labeled ubiquitin at 30 °C collected using the sequences shown in Fig. 1. Half the number of contours have been drawn in the case of the double-quantum spectra for ease in visualization. (B) Representative fits of DQ datasets for coherences of various classes (see Table 1): class I (black—Ala46, C^{α}–C^{β}), class II (red—Ile30, $C^{\gamma 1}$–$C^{\delta 1}$), and class III (blue—Leu50, C^{γ}–$C^{\delta 1}$). Circles depict the experimental data points and the calculated fits to Eq. (6) are indicated by solid lines. The data points are normalized for unit intensity at $\tau_M = 0$. Similar fits are obtained for the corresponding ZQ datasets. (C) Large differences between the decay rates of ZQC and DQC indicate the presence of exchange contributions as shown by the more rapid decay of the Leu50, C^{γ}–$C^{\delta 1}$ ZQC (red) compared with the corresponding DQC (black).

determined in this fashion were *identical* within error to those obtained without use of an offset. For the coherences used in the final analysis (vide infra) the offset was determined to be $-2.02\% \pm 1.08\%$. A similar analysis for the DQ datasets revealed an offset of $0.45\% \pm 0.32\%$ (no differences in either the rates or their errors were seen compared to fits without the offset term). Errors in the measured $\Gamma_{\mathrm{ZQ,DQ}}$ and $J_{\mathrm{ZQ,DQ}}$ represent the random errors obtained from experimental noise. In all, 38 sets of DQC/ZQC pairs were analyzed after excluding overlapping resonances and those whose intensities could not be obtained to >95% accuracy due to large errors in peak fitting. Representative spectra and fits to Eq. (6) are shown in Fig. 2.

4. Results and discussion

4.1. Theoretical framework for the estimation of $\Delta\Gamma$

To perform a separation of the effects of "conventional" relaxation from the effects of conformational exchange in the measured $\Delta\Gamma$ it was necessary to estimate the effects of the first three terms in Eq. (5). To estimate the first term corresponding to CSA/CSA cross-correlation accurately, estimates of the $^{13}C^{\mathrm{methyl}}$ and $^{13}C^{\mathrm{next}}$ shift tensors were required. Recent solid-state NMR work by Wylie et al. [34] on the protein GB1 revealed a significant amount of variability in the tensor values for various sidechain ^{13}C positions. In the present work, we assumed that both the $^{13}C^{\mathrm{methyl}}$ and $^{13}C^{\mathrm{next}}$ shift tensors were axially symmetric and their principal axes were collinear. The CSA values were estimated using $\Delta\sigma = \sigma_{33} - \frac{\sigma_{11}+\sigma_{22}}{2}$, where σ_{33} was the most downfield shifted component of the CSA tensor. Average values for a given ^{13}C position for each residue type from Wylie et al. [34] were utilized. For Leu residues (none present in GB1) we used values from Val carbons at corresponding branch points. A τ_c value of 3.5 ns was used [26,35]. Local motion was assumed to be isotropic and the unique order parameter for this interaction $S^2_{ij} = S^2_{\mathrm{CSA}}$ was assumed to be 0.80. Thus the CSA/CSA cross-correlation contributions were found to be $0.591\ \mathrm{s}^{-1}$ (Ala), $0.618\ \mathrm{s}^{-1}$ (Thr), $0.233\ \mathrm{s}^{-1}$ (Val, Leu), $0.306\ \mathrm{s}^{-1}$ (Ile, $C^{\gamma 1}$–$C^{\delta 1}$) and $0.255\ \mathrm{s}^{-1}$ (Ile, C^{β}–$C^{\gamma 2}$) at 600 MHz. The third term in Eq. (5) was calculated assuming a $C^{\mathrm{next}}C^{\mathrm{methyl}}$ bond-length of 1.527 Å and $S^2_{IS} = 0.8$ yielding a value of $0.081\ \mathrm{s}^{-1}$. Thus, the combined effect of these two terms was small and in the absence of conformational exchange, the largest contribution came from the second term in Eq. (5).

The contribution of the second term comes from four different types of interactions

(i) Dipole–dipole cross-correlation involving the $C^{\mathrm{next}}H^{\mathrm{methyl}}$ and $C^{\mathrm{methyl}}H^{\mathrm{methyl}}$ dipolar interactions, where H^{methyl} represents a methyl proton attached to C^{methyl}.
(ii) $C^{\mathrm{next}}H^{\mathrm{next}}$ and $C^{\mathrm{methyl}}H^{\mathrm{next}}$ dipole–dipole cross-correlations where H^{next} represents a proton attached to C^{next}.
(iii) $C^{\mathrm{next}}H^{\mathrm{methyl,\ remote}}$ and $C^{\mathrm{methyl}}H^{\mathrm{methyl,remote}}$ dipole–dipole cross-correlations, where $H^{\mathrm{methyl,remote}}$ represents a remote methyl proton.
(iv) $C^{\mathrm{next}}H^{k,\ \mathrm{remote}}$ and $C^{\mathrm{methyl}}H^{k,\ \mathrm{remote}}$ dipole–dipole cross-correlations, where $H^{k,\mathrm{remote}}$ represents a remote non-methyl proton.

These interactions were considered separately since the dynamic averaging due to local motion and hence $S^2_{k,\mathrm{cross}}$ in Eq. (5) was different in each case. It is to be noted that the relevant dynamical modes affecting the difference in the relaxation rates of the ZQ and DQ coherences involve motion of the $C^{\mathrm{next}}H^k$ and $C^{\mathrm{methyl}}H^k$ dipolar vectors (due to any displacement of the position of H^k, where H^k is a local or a remote proton) and the motion of the $C^{\mathrm{next}}C^{\mathrm{methyl}}$ bond itself.

The cross-correlation order parameter $S^2_{k,\mathrm{cross}}$ for the dipolar interactions of C^{next} and C^{methyl} with the same proton H^k (where H^k is either H^{methyl} or H^{next}), i.e., for interactions of types (i) and (ii) above assuming motional averaging about a single axis (C_{axis}) may be written as [36]

$$\begin{aligned} S^2_{k,\mathrm{cross}} &= S^2_{\mathrm{axis}}[a_0\Phi_0(\infty) + a_1\Phi_1(\infty) + a_2\Phi_2(\infty)], \\ a_0 &= P_2(\cos\theta_{nk})P_2(\cos\theta_{mk}), \\ a_1 &= 3\cos\theta_{nk}\cos\theta_{mk}\sin\theta_{nk}\sin\theta_{mk}\cos(\varphi_{nk} - \varphi_{mk}), \\ a_2 &= \frac{3}{4}\sin^2\theta_{nk}\sin^2\theta_{mk}\cos(2\varphi_{nk} - 2\varphi_{mk}). \end{aligned} \tag{7}$$

The orientations of the $C^{\mathrm{next}}H^k$ and $C^{\mathrm{methyl}}H^k$ dipolar vectors in a fixed reference frame are given by $\{\theta_{nk}, \varphi_{nk}\}$ and $\{\theta_{mk}, \varphi_{mk}\}$, respectively. $\Phi_0(\infty)$, $\Phi_1(\infty)$ and $\Phi_2(\infty)$ represent the limiting values of the three components of the local motional correlation function. Eq. (7) describes the motional averaging of the projection of the $C^{\mathrm{next}}H^k$ and $C^{\mathrm{methyl}}H^k$ dipolar vectors on the $C^{\mathrm{next}}C^{\mathrm{methyl}}$ axis –C_{axis} (z-axis of the reference frame) and assumes that this averaging occurs on a timescale that is much faster (by at least one order of magnitude) [37] than the motion of the C_{axis} itself (described by the order parameter S^2_{axis}). This condition is always satisfied when H^k is a methyl proton due to rapid rotations about the threefold axis (C_3).

In the simplest of models, assuming restricted diffusive motion of H^k about a single axis, the effects of any displacement of H^k may be viewed as the motion of the point of intersection between the $C^{\mathrm{next}}H^k$ and $C^{\mathrm{methyl}}H^k$ dipolar vectors (shown by the thick circle in Fig. 3A) in a circular orbit within the angular limits $\pm\gamma$ (shown in Fig. 3C). The functions $\Phi_n(\infty)$ ($n = 0, 1, 2$) in Eq. (7) are then given by [36]

$$\Phi_n(\infty) = \frac{\sin^2(n\gamma)}{(n\gamma)^2}. \tag{8}$$

In case of perfectly rigid bonds, i.e., no displacement of H^k, $\gamma = 0$ and $\Phi_0(\infty) = \Phi_1(\infty) = \Phi_2(\infty) = 1$ and Eq. (7) transforms to [36]

$$S^2_{k,\mathrm{cross}} = S^2_{\mathrm{axis}}(a_0 + a_1 + a_2) = S^2_{\mathrm{axis}}P_2(\cos\theta_{nm,k}), \tag{9}$$

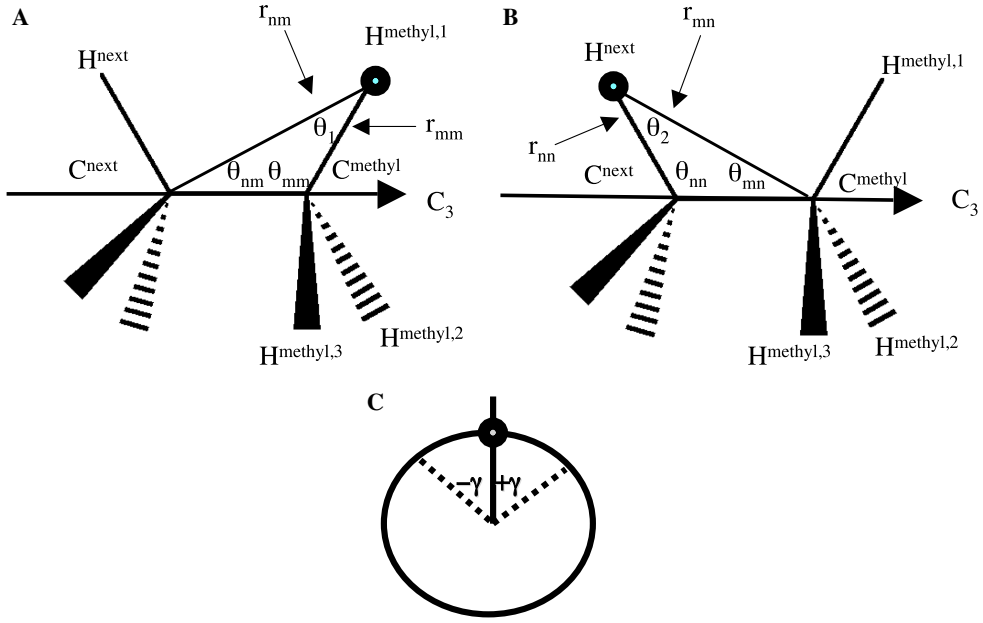

Fig. 3. Dipole–dipole interactions that affect the difference in the relaxation rates of DQC and ZQC. Cross-correlation between the dipole–dipole interactions of (A) H^{methyl} with C^{methyl} and C^{next}, (B) H^{next} with C^{methyl} and C^{next}. The C_3 axis is parallel to the $C^{next}C^{methyl}$ bond (C_3). (C) The thick circle denotes the intersection point between the $C^{next}H^k$ and $C^{methyl}H^k$ vectors, where k = methyl, next. This point moves in a circle within the angular limits of $\pm\gamma$ for any diffusive displacement of H^k. In the case of H^{methyl}, $\gamma = \pi$.

where $\theta_{nm,k}$ is the angle between the $C^{next}H^k$ and $C^{methyl}H^k$ dipolar vectors (θ_1 or θ_2 in Fig. 3). In case of unrestricted diffusion of H^k and completely disordered bond vectors, $\gamma = \pm\pi$, we have $\Phi_0(\infty) = 1$ and $\Phi_1(\infty) = \Phi_2(\infty) = 0$ thus Eq. (7) transforms to [36]

$$S^2_{k,\mathrm{cross}} = S^2_{\mathrm{axis}} P_2(\cos\theta_{nk}) P_2(\cos\theta_{mk}). \tag{10}$$

To evaluate $S^2_{k,\mathrm{cross}}$ for the interactions (i) and (ii) above, we defined the following co-ordinate system—the z-axis was defined to be collinear with the $C^{next}C^{methyl}$ bond ($C_{axis} = C_3$) with the $C^{next}C^{methyl}$ and $C^{methyl}H^{methyl,1}$ vectors lying in the xz-plane. The coefficients in Eq. (7) were found to be $a_0 = -0.22$, $a_1 = 0.39$, and $a_2 = 0.15$. In the case, where H^k is H^{methyl}, Eq. (10) holds due to rapid rotation of the methyl group about the $C^{next}C^{methyl}$ (C_3) axis. When H^k is H^{next}, $S^2_{k,\mathrm{cross}}$ is evaluated using Eqs. (7) and (8) in the general case.

We take a more empirical approach to evaluating terms of type (iii) and (iv) described above. For interactions of type (iii) we assume averaging of the remote methyl proton about its *own* C_3 (C'_3—this defines the z-axis of the co-ordinate frame) axis and utilize Eq. (10) replacing the order parameter S^2_{axis} by $S^2_{k,\mathrm{remote}} = S^2_{\mathrm{axis}} S^2_{\mathrm{axis,remote}}$. The additional scaling represented by $S^2_{\mathrm{axis,remote}}$ is included to account for motion of the C'_3 axis itself in an empirical fashion and S^2_{axis} represents the motion experienced C^{next} and C^{methyl} nuclei since the local C_3 axis is collinear with the $C^{next}C^{methyl}$ bond and local motion has been assumed to be isotropic in the analysis adopted here. $S^2_{\mathrm{axis,remote}}$ is taken to be 0.9 when the remote methyl proton is on the same residue and 0.7 otherwise. In the case of remote non-methyl protons, we used Eq. (9) with S^2_{axis} replaced by $S^2_{k,\mathrm{remote}} = S^2_{\mathrm{axis}} S^2_{\mathrm{axis,remote}}$ with $S^2_{\mathrm{axis,remote}}$ taking values of 0.7 or 0.9 as before and $\theta_{nm,k}$ is replaced by $\theta_{nm,k,\mathrm{remote}}$. Remote protons that were more than 5 Å away from *both* the C^{next} and C^{methyl} nuclei that constitute the ZQC and DQC were excluded from the analysis. Formally, for remote interactions, the r_{IH^k} and r_{SH^k} in Eq. (5) may also be time-dependent and this would require the definition of a radial order parameter in addition to the traditional angular order parameters described above. However these additional effects are expected to be minimal.

In the absence of chemical exchange the largest contributions (>90%) to Eq. (5) involved dipole–dipole cross-correlations involving local protons, i.e., protons connected to C^{next} or C^{methyl} nuclei forming the ZQC/DQC. However our estimates of all terms in Eq. (5) were used in the present analysis.

4.2. Analysis of the relaxation rates

The average values and standard deviations for Γ_{DQ} and Γ_{ZQ} for ^{15}N, ^{13}C-labeled ubiquitin at 30 °C were found to be $31.09 \pm 7.44\ s^{-1}$ and $35.33 \pm 11.10\ s^{-1}$, respectively (shown in Table 2) and the J_{DQ} and J_{DQ} were found to 33.88 ± 6.02 Hz and 34.00 ± 5.77 Hz, respectively (data not shown since these were not analyzed further). The reproducibility of the measured values was confirmed and the random errors determined from four independent sets of measurements obtained over a period of 6 weeks.

Using the theoretical framework described above and utilizing the cluster of 10 NMR structures of ubiquitin (PDB reference code—1D3Z) we estimated contributions from the first three terms in Eq. (5). In almost all of the cases the

Table 2
Measured ZQC and DQC relaxation rates in ^{13}C, ^{15}N-labeled ubiquitin at 30 °C[a]

Coherence	Γ_{DQ} (s^{-1})	$\Delta\Gamma_{DQ}$ (s^{-1})	Γ_{ZQ} (s^{-1})	$\Delta\Gamma_{ZQ}$ (s^{-1})	$\Delta\Gamma=\Gamma_{DQ}-\Gamma_{ZQ}$ (s^{-1})	$\Delta\Delta\Gamma$ (s^{-1})
Ile3,$C^{\gamma1}$–$C^{\delta1}$	34.4	0.1	40.6	1.8	−6.3	1.8
Ile3,C^{β}–$C^{\gamma2}$	38.2	0.2	43.8	1.1	−5.6	1.1
Val5,C^{β}–$C^{\gamma2}$	31.8	0.9	33.7	0.7	−1.9	1.1
Thr7,C^{β}–$C^{\gamma2}$	18.8	0.1	19.9	0.4	−1.1	0.4
Leu8,C^{γ}–$C^{\delta1}$	23.9	0.7	19.6	<0.1	4.3	0.7
Thr9,C^{β}–$C^{\gamma2}$	23.7	0.4	24.3	0.1	−0.6	0.4
Thr12,C^{β}–$C^{\gamma2}$	26.4	0.6	28.5	0.9	−2.1	1.1
Ile13,$C^{\gamma1}$–$C^{\delta1}$	25.4	0.1	30.5	0.1	−5.1	0.1
Ile13,C^{β}–$C^{\gamma2}$	30.9	0.3	33.7	1.2	−2.8	1.2
Thr14,C^{β}–$C^{\gamma2}$	25.4	0.2	26.7	0.9	−1.4	0.9
Leu15,C^{γ}–$C^{\delta1}$	29.7	0.8	42.3	1.7	−12.7	1.9
Val17,C^{β}–$C^{\gamma1}$	35.6	0.8	37.8	0.2	−2.2	0.8
Val17,C^{β}–$C^{\gamma2}$	35.7	0.1	37.9	0.5	−2.2	0.6
Thr22,C^{β}–$C^{\gamma2}$	17.3	0.2	18.3	0.4	−1.0	0.4
Ile23,$C^{\gamma1}$–$C^{\delta1}$	31.9	0.4	35.2	0.5	−3.3	0.6
Ile23,C^{β}–$C^{\gamma2}$	43.7	1.2	43.2	0.9	0.4	1.5
Val26,C^{β}–$C^{\gamma1}$	33.9	0.1	35.5	0.1	−1.6	0.1
Val26,C^{β}–$C^{\gamma2}$	27.6	0.1	28.2	0.3	−0.6	0.3
Ile30,$C^{\gamma1}$–$C^{\delta1}$	41.3	0.2	47.6	0.9	−6.3	0.9
Ile30,C^{β}–$C^{\gamma2}$	38.3	0.6	45.0	0.1	−6.7	0.6
Ile36,$C^{\gamma1}$–$C^{\delta1}$	30.3	0.7	32.4	0.6	−2.1	1.0
Ile36,C^{β}–$C^{\gamma2}$	31.2	0.1	33.8	1.2	−2.6	1.2
Leu43,C^{γ}–$C^{\delta1}$	33.4	0.3	38.2	0.7	−4.8	0.7
Ile44,$C^{\gamma1}$–$C^{\delta1}$	21.7	0.3	21.5	0.4	0.3	0.4
Ile44,C^{β}–$C^{\gamma2}$	35.5	0.5	41.5	0.9	−6.1	1.0
Ala46,C^{α}–C^{β}	24.0	0.4	31.2	1.8	−7.2	1.9
Leu50,C^{γ}–$C^{\delta1}$	35.9	2.7	53.6	5.2	−17.7	5.9
Leu50,C^{γ}–$C^{\delta2}$	46.9	1.1	60.6	1.0	−13.8	1.5
Thr55,C^{β}–$C^{\gamma2}$	28.9	0.3	30.0	2.1	−1.1	2.1
Leu56,C^{γ}–$C^{\delta1}$	30.4	0.1	42.3	0.7	−12.0	0.7
Leu56,C^{γ}–$C^{\delta2}$	44.4	0.1	67.2	2.1	−22.8	2.2
Ile61,$C^{\gamma1}$–$C^{\delta1}$	33.1	0.4	33.8	0.1	−0.8	0.4
Ile61,C^{β}–$C^{\gamma2}$	37.3	0.1	40.9	1.1	−3.6	1.1
Leu67,C^{γ}–$C^{\delta1}$	28.2	0.1	29.9	<0.1	−1.7	0.1
Leu67,C^{γ}–$C^{\delta2}$	28.4	0.1	30.2	<0.1	−1.9	0.1
Leu71,C^{γ}–$C^{\delta1}$	22.4	0.4	24.2	0.6	−1.8	0.7
Leu73,C^{γ}–$C^{\delta1}$	21.7	0.4	23.3	0.7	−1.6	0.8
Leu73,C^{γ}–$C^{\delta2}$	21.2	1.1	21.4	0.2	−0.2	1.1

[a] $\Delta\Gamma_{ZQ,DQ}$ denote the random errors in the $\Gamma_{ZQ,DQ}$ values. Rates determined from time-points $\tau_M \leqslant 28$ ms (see text). $\Delta\Delta\Gamma=\sqrt{\Delta\Gamma_{DQ}^2+\Delta\Gamma_{ZQ}^2}$ represents the errors in the $\Delta\Gamma$ values.

measured $\Delta\Gamma=\Gamma_{DQ}-\Gamma_{ZQ}$ could be explained without the need to invoke the presence of slow conformational exchange represented by the fourth term in Eq. (5), i.e., R^{ex}. As previously stated, the dominant effect on $\Delta\Gamma$ came from the second term in Eq. (5). The largest contribution to this term results from dipolar interactions with H^{methyl} and H^{next} namely interactions of the type (i) and (ii) mentioned in the theoretical framework above. The contribution of these two types of interactions merits some detailed attention. Taking account of the fact that there are 3 H^{methyl} and 1 H^{next} (2 for ZQC/DQC involving Ile $C^{\delta1}$) the expected contributions of these two effects to $\Delta\Gamma(\Delta\Gamma^{dd}_{local})$ can be written as

$$\Delta\Gamma^{dd}_{local}=2\left(\frac{2}{5}\tau_c\right)\left(\frac{\mu_0\hbar}{4\pi}\right)^2\frac{\gamma_H^2\gamma_C^2}{r_1^3r_2^3}\left[3S^2_{axis}P_2(\cos\theta_{nm})P_2(\cos\theta_{mm})+nS^2_{k,cross}\right], \quad (11)$$

where r_1 is either r_{mm} or r_{nn} (Figs. 3A and B), i.e., the CH bond-length (taken to be 1.09 Å) and r_2 is either r_{nm} or r_{mn} (taken to be 2.15 Å) and θ_{nm} and θ_{mm} are shown in Figs. 3A and B, and $S^2_{k,cross}$ is given by Eqs. (7) and (8). $n=2$ for coherences involving Ile $C^{\delta1}$ and $n=1$ for all other cases. Using $\tau_c=3.5$ ns as suggested by Lee et al. [26,35] (this value of τ_c was used by Lee and Wand to extract the S^2_{axis} values from ^2H relaxation data and the S^2_{axis} values obtained by them have been utilized in the present analysis) and representative structures from the NMR cluster, the contribution of the first term within the brackets in Eq. (11) to the quantity $\Delta\Gamma^{dd}_{local}/S^2_{axis}$ was found to be $-5.17\ s^{-1}$. Note that $\Delta\Gamma^{dd}_{local}/S^2_{axis}$ depends on the amount of motional restriction of the $C^{next}H^{next}$ bond, i.e., on the angle γ, through its contribution to the second term within brackets in Eq. (11). It is possible to estimate $\Delta\Gamma^{dd}_{local}/S^2_{axis}$ using various degrees of motional restriction of the $C^{next}H^{next}$ bond, i.e., with different values of γ. $\Delta\Gamma^{dd}_{local}/S^2_{axis}=-2.67\ s^{-1}$ for completely restricted motion of the $C^{next}H^{next}$ bond, i.e., $\gamma=0°$ with a contribution of $2.51\ s^{-1}$ from second term within the brackets in Eq. (11). For unrestricted motion (completely free diffusive motion of H^{next}) of the $C^{next}H^{next}$ bond ($\gamma=180°$) these values are -6.90 and $-1.72\ s^{-1}$. For ZQC/DQC involving the Ile $C^{\gamma1}$–$C^{\delta1}$ coherence (there are two γ_1 protons in Ile) the values for $\gamma=0$: -0.16 and $5.02\ s^{-1}$; $\gamma=180$: -8.62 and $-3.45\ s^{-1}$. Thus in our single axis diffusion model, small values of $\Delta\Gamma^{dd}_{local}/S^2_{axis}$ indicate restricted motion of the $C^{next}H^{next}$ bond since the two terms in Eq. (11) interfere destructively being opposite in sign. Under these circumstances the errors caused by the empirical treatment of the CSA–CSA cross-correlation and dipole–dipole cross-correlations involving remote protons (interactions of types (iii) and (iv) discussed above) may be exacerbated. In this limit, an auto-correlated relaxation rate involving the $C^{next}H^{next}$ dipolar interaction, when available, is expected to be a better reporter of local dynamics than the cross-correlated rates measured in the present case (see Appendix B).

We utilized the S^2_{axis} values reported from ^2H relaxation measurements by Lee et al. [26] and the theoretical framework described above to obtain the scaled difference between the ZQ and DQ relaxation rates ($\Delta\Gamma/S^2_{axis}$) involving 38 methyl groups in ubiquitin (Fig. 4). Calculated $\Delta\Gamma$ values included our estimates *all the terms* in Eq. (5). These values were then compared with the experimental $\Delta\Gamma/S^2_{axis}$ values to estimate the degree of motional restriction (denoted by the angle γ) of the $C^{next}H^{next}$ bond (actually in true mathematical terms we are determining the degree to which the H^{next} nucleus diffuses about its equilibrium position—in physico-chemical terms this corresponds to the motional restriction of the $C^{next}H^{next}$ bond) using Eqs. (7) and (8). We generated expected $\Delta\Gamma/S^2_{axis}$ on a grid of γ values from 0° to 180° in 10° increments. We felt that using a finer grid would not be justified since the estimates of the first and third terms in Eq. (5) and contributions of the interactions of types (iii) and (iv) to the second term are

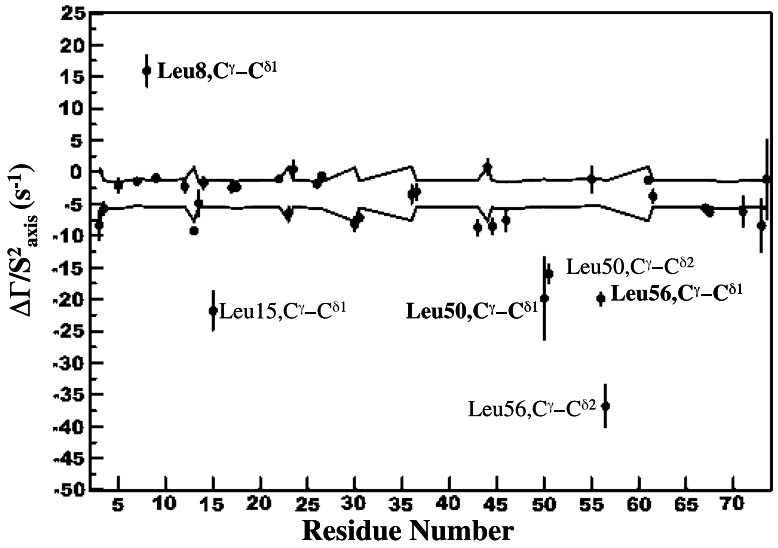

Fig. 4. Experimental values of $\Delta\Gamma/S^2_{\text{axis}}$ are indicated by the filled circles and calculated values by the solid lines assuming either completed restricted (upper line, $\gamma = 0°$) or a completely disordered (lower line, $\gamma = 180°$) of the $C^{\text{next}}H^{\text{next}}$ bond vector using the single axis diffusion model. S^2_{axis} values obtained from the ^{2}H relaxation measurements of Lee et al. [26] have been utilized to calculate $\Delta\Gamma/S^2_{\text{axis}}$ values. ZQC/DQC with exchange contributions to the $\Delta\Gamma/S^2_{\text{axis}}$ values (see text) are labeled in boldface.

only approximate. The estimated γ values are summarized in Table 3.

For Thr residues, the estimated γ values lie between 10° and 30° representing a high degree of order of the C^{β}–H^{β} bond vector. It is to be mentioned here that S^2_{axis} values for these residues are 0.83 ± 0.13 representing a high degree of order of the methyl symmetry (C_3) axis corresponding to the C^{β}–$C^{\gamma 2}$ bond. Note that the γ values and S^2_{axis} values report on the motion of two almost orthogonal vectors and discrepancies between these values may be due to the presence of complex anisotropic local motional modes as reported by Fischer et al. [3] in the protein backbone and discussed for sidechains in some detail by Yang et al. [27]. The calculated γ value Thr9 seems to indicate a marginally higher degree of order than expected from the S^2_{axis} value. This could be due to several reasons, including the presence of anisotropic fast motional modes or the presence of a slow dynamic mode that contributes a positive R^{ex} (vide infra) to $\Delta\Gamma$ that increases its overall value and leads to a smaller value of γ. The latter scenario seems more likely in the present case since Leu8 (see below) contains a significant R^{ex} contribution. A similar high degree of order is seen for Val residues with γ values between 0° and 40° and S^2_{axis} values (corresponding to the motion of the $C^{\beta}C^{\gamma 1,2}$ bonds) given by 0.81 ± 0.23.

In considering the relaxation properties of C^{γ}–$C^{\delta 1,2}$ coherences in Leu residues one has to consider the effects of strong coupling due to possible chemical shift degeneracy between C^{γ} and $C^{\delta 1,2}$ nuclei. The extent of strong coupling can be described a parameter $\theta = \frac{1}{2}\tan^{-1}(\frac{J_{CC}}{\delta_{\gamma}-\delta_{\delta}})$ [38], where δ_{γ} and δ_{γ} are the chemical shifts of the C^{γ} and $C^{\delta 1,2}$, respectively. A θ value $<5°$ ($\cos\theta > 0.99$) may be considered weak coupling and a $\theta > 25°$ ($J_{CC} \approx \delta_{\gamma} - \delta_{\delta}$) may be considered very strong coupling. It is notable that in the limit of very strong coupling *there are no additional contributions* to $\Delta\Gamma$ values when compared with the weak-coupling limit [38]. However, the following situation requires a careful attention—consider the scenario where C^{γ} is degenerate with $C^{\delta 1}$ (downfield C^{δ}), while $C^{\delta 2}$ (upfield C^{δ}) is far enough upfield that it is in the weak-coupling limit with respect to C^{γ}. In such a case, when considering the C^{γ}–$C^{\delta 1}$ ZQ/DQ coherence (involving the very strongly coupled spins), we may simply consider evolution under a weak coupling with $C^{\delta 2}$ as represented by Eq. (6). However, since C^{γ} and $C^{\delta 1}$ are strongly coupled we cannot generate a pure C^{γ}–$C^{\delta 2}$ coherence without mixing in $C^{\delta 1}$ and the dynamics of the C^{γ}–$C^{\delta 2}$ coherence would be rather complex and not accurately represented by Eq. (6). Thus, in the present work we only consider only those Leu coherences where the θ value either $<5°$ for *both* C^{δ}s or only the coherence that involves a C^{δ} *that is strongly coupled* with the corresponding C^{γ} ($\theta > 25°$). Thus, coherences corresponding to Leu15 and Leu43 were not analyzed further. For Leu residues, the S^2_{axis} values in ubiquitin are quite low 0.25 ± 0.06 and this is reflected in the γ values which lie between 90° and 180° for the $C^{\gamma}H^{\gamma}$ bond. The Leu73 C^{γ}–$C^{\delta 1}$ bond seems to be better ordered than predicted by the S^2_{axis} value but the error in γ is very large and the upper and lower bounds of γ in this case cover the full range of possible γ values. However, the situation is rather complicated for the Ile residues with rather poor correlation between S^2_{axis} values of Lee et al. and the γ values obtained from the present study.

Fig. 5 shows the comparison of the γ values obtained in the present study with the S^2_{axis} values obtained by Lee et al. [26]. The errors in γ values are generally quite large, this is a reflection of the fact that the quantities that are directly measured are the $\Gamma_{\text{DQ,ZQ}}$ values and the individual errors

Table 3
Motional restriction of the C^{next}–H^{next} bond[a]

Bond-vector ($C^{next}H^{next}$)	Coherence (C^{next}–C^{methyl})	γ^{o}[b]	S^2_{axis}[c]
Thr			
Thr7,C^{β}–H^{β}	C^{β}–$C^{\gamma 2}$	20 ± 20	0.75
Thr9,C^{β}–H^{β}	C^{β}–$C^{\gamma 2}$	10 ± 10	0.64
Thr12,C^{β}–H^{β}	C^{β}–$C^{\gamma 2}$	30 ± 40	0.93
Thr14,C^{β}–H^{β}	C^{β}–$C^{\gamma 2}$	20 ± 30	0.78
Thr22,C^{β}–H^{β}	C^{β}–$C^{\gamma 2}$	10 ± 10	0.95
Thr55,C^{β}–H^{β}	C^{β}–$C^{\gamma 2}$	30 ± 40	0.93
Val			
Val5,C^{β}–H^{β}	C^{β}–$C^{\gamma 2}$	30 ± 30	0.88
Val17,C^{β}–H^{β}	C^{β}–$C^{\gamma 1}$	40 ± 20	0.89
Val17,C^{β}–H^{β}	C^{β}–$C^{\gamma 2}$	40 ± 20	0.89
Val26,C^{β}–H^{β}	C^{β}–$C^{\gamma 1}$	20 ± 10	0.86
Val26,C^{β}–H^{β}	C^{β}–$C^{\gamma 2}$	0 ± 10	0.99
Leu			
Leu67,C^{γ}–H^{γ}	C^{γ}–$C^{\delta 1}$	160 ± 20	0.30
Leu67,C^{γ}–H^{γ}	C^{γ}–$C^{\delta 2}$	180 ± 10	0.29
Leu71,C^{γ}–H^{γ}	C^{γ}–$C^{\delta 1}$	120 ± 40	0.29
Leu73,C^{γ}–H^{γ}	C^{γ}–$C^{\delta 1}$	140 ± 40	0.19
Leu73,C^{γ}–H^{γ}	C^{γ}–$C^{\delta 2}$	90 ± 90	0.17
Ile			
Ile3,$C^{\gamma 1}$–$H^{\gamma 1}$	$C^{\gamma 1}$–$C^{\delta 1}$	140 ± 40	0.75
Ile13,$C^{\gamma 1}$–$H^{\gamma 1}$	$C^{\gamma 1}$–$C^{\delta 1}$	180 ± 10	0.55
Ile23,$C^{\gamma 1}$–$H^{\gamma 1}$	$C^{\gamma 1}$–$C^{\delta 1}$	120 ± 40	0.51
Ile30,$C^{\gamma 1}$–$H^{\gamma 1}$	$C^{\gamma 1}$–$C^{\delta 1}$	150 ± 30	0.77
Ile36,$C^{\gamma 1}$–$H^{\gamma 1}$	$C^{\gamma 1}$–$C^{\delta 1}$	70 ± 20	0.58
Ile44,$C^{\gamma 1}$–$H^{\gamma 1}$	$C^{\gamma 1}$–$C^{\delta 1}$	10 ± 20	0.31
Ile61,$C^{\gamma 1}$–$H^{\gamma 1}$	$C^{\gamma 1}$–$C^{\delta 1}$	40 ± 10	0.56
Ile3,C^{β}–H^{β}	C^{β}–$C^{\gamma 2}$	140 ± 40	0.98
Ile13,C^{β}–H^{β}	C^{β}–$C^{\gamma 2}$	110 ± 40	0.56
Ile23,C^{β}–H^{β}	C^{β}–$C^{\gamma 2}$	0 ± 10	0.95
Ile30,C^{β}–H^{β}	C^{β}–$C^{\gamma 2}$	180 ± 10	0.93
Ile36,C^{β}–H^{β}	C^{β}–$C^{\gamma 2}$	60 ± 40	0.83
Ile44,C^{β}–H^{β}	C^{β}–$C^{\gamma 2}$	180 ± 10	0.71
Ile61,C^{β}–H^{β}	C^{β}–$C^{\gamma 2}$	80 ± 40	0.95

[a] Coherences with R^{ex} contributions not shown. Ala46 which has been determined to have R^{ex} contributions by comparison with other measurements (see text) is also not shown.
[b] Error bounds in γ calculated from the $\Delta\Delta\Gamma S^2_{axis}$ values.
[c] S^2_{axis} values taken from Lee et al. [26].

are propagated into the $\Delta\Gamma$ values. These errors and the errors in S^2_{axis} from Lee et al. are further propagated to calculate $\Delta\Gamma/S^2_{axis}$ values and ultimately γ values. The boxed areas display regions of different motional restriction—residues with $0^0 \leqslant \gamma \leqslant 60^0$ are considered to be highly ordered, $60^0 < \gamma \leqslant 120^0$ are considered to be partially ordered and $\gamma > 120^0$ are considered to be highly disordered. The corresponding classification for the S^2_{axis} values are $S^2_{axis} \geqslant 0.7$, $0.7 > S^2_{axis} \geqslant 0.5$, and $S^2_{axis} < 0.5$. Thus the points enclosed within or near the boxed regions show good qualitative agreement between S^2_{axis} and γ values. It is evident from Fig. 5 that most coherences except a large number corresponding to Ile residues (shown in blue) show qualitative agreement between the two sets of values. It is perceivable that some of the discrepancies may arise from anisotropic local motion or from an empirical treatment of interactions of type (iii) and (iv). However, extremely large differences as seen in the following coherences—Ile3, $C^{\gamma 1}$–$H^{\gamma 1}$; Ile30, $C^{\gamma 1}$–$H^{\gamma 1}$; Ile44, $C^{\gamma 1}$–$H^{\gamma 1}$; Ile3, C^{β}–H^{β}; Ile30, C^{β}–H^{β}; and Ile44, C^{β}–H^{β}. For these coherences that lie in protein core, the extremely large discrepancies between the S^2_{axis} and γ values cannot be explained merely by anisotropic motional effects alone and point to a failure in our choice of motional models.

It is therefore likely that more complicated motional models (see Appendix C) and the inclusion of the possibility of correlated motion about multiple axes may be necessary to accurately analyze the measured cross-correlation rates for residues in the tightly packed protein central core, though simple motional models may suffice for shorter chain amino acids and for residues that lie in the fringes of the protein. These complex motional effects may become critical for longer and asymmetrically branched amino acids (Ile > Leu > Val). Also, motional correlations are expected to be more likely in better-ordered systems and less where there is more disorder. Restricted diffusion models may not be the only possible motional models that could be appropriate to interpret the measured cross-correlation rates. It has been shown through molecular dynamics (MD) simulations that jump models with restricted diffusion within minima that take into account transitions between rotameric states [39] as well as motional restriction within these states (see Appendix C) may be necessary in certain cases. It is to be noted that these conformational transitions may often be quite slow compared to the rotational correlation time and may not affect S^2_{axis} values (they are thus not fast motions in the true sense and may or may not result in slow modulation of isotropic chemical shifts leading to R^{ex} contributions discussed below), however they will affect the interpretation of the cross-correlations rates in the present case and order parameters obtained from scalar couplings or residual dipolar coupling values as shown by Chou et al. [40]. Evidence of rotamer averaging for Ile3, Ile30, and Ile44 has been noted by Chou et al. [40]. Further, an inspection of the recent dynamically refined (DER—dynamic ensemble refinement) structural ensemble of ubiquitin (PDB code—1XQQ) presented by Lindorff-Larsen et al. [41] revealed that these three residues exhibit a far greater amount of disorder about the χ_1 and χ_{21} angles when compared with the structures used in the present analysis (PDB code—1D3Z). This is especially pronounced in case of the Ile44 χ_1 angle.

In some residues such as Val17, Val26, Leu67, and Leu73 there are two independent measurements of the motional restriction of the same bond-vector $C^{\beta}H^{\beta}$ in Val (measured from the C^{β}–$C^{\gamma 1}$ and C^{β}–$C^{\gamma 2}$ coherences) and $C^{\gamma}H^{\gamma}$ in Leu (measured from C^{γ}–$C^{\delta 1}$ and C^{γ}–$C^{\delta 2}$ coherences). As is evident from Table 3, the results are consistent is all cases except for Leu73 which has an extremely large uncertainty in the calculated γ value in the case of the $C^{\gamma}C^{\delta 1}$ coherence.

Three Leu residues (after excluding the ones with complex dynamics as discussed above) involving the following coherences: Leu8—C^{γ}–$C^{\delta 1}$; Leu50—C^{γ}–$C^{\delta 1}$; and Leu56—C^{γ}–$C^{\delta 1}$ display extremely large absolute values of $\Delta\Gamma$.

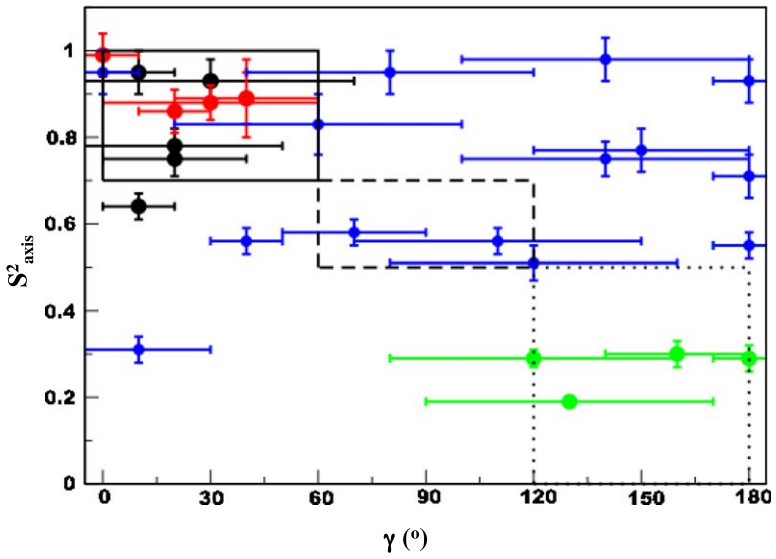

Fig. 5. Plots of the motional restriction of the $C^{next}H^{next}$ vector represented by the γ values against the motional restriction of the $C^{next}C^{methyl}$ (C_3) axis represented by the S^2_{axis} values of Lee et al. [26]. Thr (black), Val (red), Leu (green), and Ile (blue) residues are depicted. Smaller circles are used for Ile residues for visual convenience only. The solid lines enclose the region corresponding to $0^0 \leqslant \gamma \leqslant 60^0; 0.7 \leqslant S^2_{axis}$ (signifying a high degree of motional restriction), the dashed lines enclose the region corresponding to $60^0 < \gamma \leqslant 120^0; 0.7 > S^2_{axis} \geqslant 0.5$ (signifying intermediate motional restriction) and the dotted lines enclose the region corresponding to $120^0 < \gamma; 0.5 > S^2_{axis}$ (signifying a limited amount of motional restriction or a high degree of disorder). The experimental points lying within (or close to) the boxed regions denote qualitative agreement between the γ and the S^2_{axis} values. Errors in γ values are obtained by simple propagation of the measured $\Gamma_{ZQ,DQ}$ errors and the errors in S^2_{axis} are from Lee et al. [26]. The Leu73 C^{γ}–$C^{\delta 1}$ coherence, which has an extremely large error covering the whole range of γ values is not shown.

These values may be accounted for by the inclusion of exchange contributions resulting from μs–ms timescale motion, i.e., inclusion of an R^{ex} term in Eq. (5). These residues belong in regions that show significant exchange contributions in the relaxation of ZQC and DQC involving both backbone [21] and sidechain [23] nuclei. In fact, a recent study of the relaxation properties of ZQC and DQC involving $^{13}C^{\alpha}$ and $^{13}C^{\beta}$ nuclei in ubiquitin revealed that the largest contribution from exchange processes occurred in Leu50 and Leu56 [23]. In the present case, for Leu50 and Leu56, the modulation of the isotropic chemical shifts for the C^{γ} and $C^{\delta 2}$ nuclei are anti-correlated (an upfield shift in one and a downfield shift in the other) leading to a negative value of the R^{ex} term (fourth term in Eq. (5)) and a negative contribution towards $\Delta\Gamma$. On the other hand, for the C^{γ}–$C^{\delta 1}$ coherence in Leu8, the shifts are correlated (downfield or upfield shifts for both nuclei) leading to a positive R^{ex} contribution. For the only Ala residue we could analyze, namely Ala46, we found that the $\Delta\Gamma$ ($\Delta\Gamma/S^2_{axis}$) value could be explained wholly by the presence of motion on the ps–ns timescale. The results of our analysis indicated that the motional restriction of the C^{α}–H^{α} bond was completely unrestricted ($\gamma = 180°$). This contradicts previous results on fractionally ^{13}C-labeled ubiquitin [42] which showed that the S^2 value for the C^{α}–H^{α} bond was 0.81. It is therefore likely that an elevated absolute value of $\Delta\Gamma$ may be the result of a contribution from conformational exchange (negative contribution of R^{ex} and anti-correlated shift changes). This residue lies in a region which has been previously shown to display slow dynamics (notably Phe45) [21,23]. This effect may also contribute to the discrepancy seen in Ile44, above. It should be noted that even though a large majority of $\Delta\Gamma/S^2_{axis}$ values described above could be completely described without the need to include a R^{ex} term in Eq. (5), however the possibility that some of these rates may contain exchange contributions, may not be completely eliminated. Indeed, the effects of

Fig. 6. Comparison of those residues that display slow μs–ms timescale motion for sidechains (red, present study) and those with backbone χ values less than 0.5 (blue, see text) from Majumdar and Ghose [21]. The residues with the largest effects are clustered in the same region indicating that they may all be affected by the same (yet undetermined) motional mode.

conformational exchange can have contributions to Eq. (5) that are opposite in sign to the contributions of the effects of fast motions. The most efficient method to quantitatively measure the presence of R^{ex} terms is to perform several experiments using multiple refocusing of the ZQC and the DQC terms with different inter-pulse spacing as proposed by Dittmer and Bodenhausen [29]. However, simple CPMG-type experiments for multiple-quantum coherences have been shown to fail and more elaborate multi-pulse schemes have to be employed [43]. In case of protein sidechains, an added level of complexity is the necessity to use multi-pulse sequences that employ shaped pulses for selective refocusing. We are, through simulations, investigating the best possible multi-pulse scheme to accurately measure R^{ex} terms in sidechain ZQC/DQC relaxation.

Finally, we decided to compare the residues (Leu8, Leu50, and Leu56) that undergo slow dynamics in sidechain regions (confirmed from the present study) with those that were shown to display motion on similar timescales in the backbone from our previous studies. We had defined a quantity χ that was a measure of the amount and extent (number of bonds over which the DQ or ZQ were generated) of correlated motion on the μs–ms timescale in the protein backbone [21]. This quantity was 1 for those residues that were rigid on the slow timescale and 0 for the residue that displayed the largest amount of motion on this timescale. The residues with χ values <0.5 (Glu24, Asn25, Glu51, and Asp52) from Majumdar and Ghose [21] (shown in blue) are displayed in Fig. 6 along with Leu8, Leu50, and Leu56 where motion on the slow timescales was demonstrated by the present study (shown in red). A large majority of these residues lie in the same region and are probably affected by the same motional mode. The exact nature of this mode remains to be ascertained. Leu8 lies on the turn between the first and second β-strand in a region that has been shown to display slow motion in the protein sidechain [23].

Since our estimates of the motional restriction of the $C^{next}H^{next}$ vector depends on extracting the effects of the cross-correlation between the dipolar interactions between the $C^{next}H^{next}$ and $C^{methyl}H^{next}$ dipoles while relying on estimates of the other effects contributing to $\Delta\Gamma$, knowledge of the exact nature of the CSA tensors of $^{13}C^{next}$ and $^{13}C^{methyl}$ nuclei would go far to improve the accuracy of our results. Availability of the principal values of the CSA tensor from solid-state NMR measurements [34] and the orientations from ab inito calculations [44] would improve the accuracy of these values. Accurate estimates of dipolar interactions with remote protons are also required.

The interpretation of cross-correlation effects (especially in sidechains) in terms of motional models is often more challenging in multiple-quantum coherences than in single-quantum coherence since a larger number of interactions and hence a larger number of motional modes are involved. As discussed above, the single axis diffusion model (requiring a single parameter γ to describe the motion) proves inadequate for longer chain asymmetrically branched amino acids such as Ile in the tightly packed central protein core. More complex motional models including the possibility of correlation between various motional modes are required to adequately interpret the $\Delta\Gamma$ values for these residues (see Appendix C). Such analyses require a larger number of parameters, a minimum of three for correlated two-axis diffusion, and hence a larger number of measurements with higher precision than in the present case. Further, a decoupling of the motions of the $C^{next}C^{methyl}$ (C_3) axis and the $C^{next}H^{next}$ bond vector has been assumed in deriving Eq. (5) and utilized in the subsequent analysis for the single-axis diffusion model. This assumption may also not be generally valid except in cases with very low S^2_{axis} values. The choice of physically reasonable motional models and the nature of correlation between various motional modes could in principle be obtained from an analysis of MD trajectories using either improved implicit [45] or explicit solvent models.

Acknowledgments

This work has been supported in part by a CAREER grant (MCB-0347100) from the National Science Foundation and a grant (5G12 RR03060) from the National Institutes of Health. Support from the Graduate Research and Teaching Initiative (GRTI) from the State of New York is also acknowledged. We thank Prof. Chad Rienstra of the University of Illinois Urbana-Champaign for providing us with the ^{13}C CSA values of GB1 prior to publication. We also thank Dr. Fabien Ferrage and Dr. Kaushik Dutta of the New York Structural Biology Center, and Dr. Dominique Frueh of the Harvard Medical School for useful discussions. AA has been supported by a CCAPP grant from the New York State Department of Education.

Appendix A. The secular approximation

The relaxation of the $C^{next}C^{methyl}$ DQC and ZQC is best described in the context of a 4-spin system involving two protons H^1 and H^2 which may be either remote or local. The various cross-correlated interactions that are involved in the evolution of the coherences in question may be classified into several different classes.

(i) Dipole–dipole cross-correlation of between the C^iH^j and C^kH^j dipolar interactions with $\{i,\ k = \text{methyl, next};\ i \neq k\}$ and $\{j = 1,2\}$, i.e., dipolar interactions with the same proton. This is a *secular* interaction (in either the ZQ or the DQ subspace) and leads to differential relaxation between the ZQC and DQC. This term is not affected by proton inversion or proton decoupling.

(ii) Dipole–dipole cross-correlation between the C^iH^j and C^iH^k dipolar interactions with $\{i = \text{methyl, next}\}$ and $\{j,k = 1,2; j \neq k\}$, i.e., dipole–dipole cross-correlation with the same carbon. This is a *non-secular* interaction and leads to the creation of $I_+S_+ \rightarrow 4I_+S_+H^j_zH^k_z$ and

$I_-S_- \rightarrow 4I_-S_-H_z^jH_z^k$. This interaction is also not averaged out by proton inversion or decoupling.

(iii) Dipole–dipole cross-correlation of between the C^iH^j and C^kH^l dipolar interactions with $\{i,k =$ methyl, next; $i \neq k\}$ and $\{j, l = 1,2; j \neq 1\}$. This is a *non-secular* interaction and leads to the creation of $I_+S_+ \rightarrow 4I_+S_+H_z^jH_z^l$ and $I_-S_- \rightarrow 4I_-S_-H_z^jH_z^k$. This interaction is also not averaged out by proton inversion or decoupling.

(iv) CSA-dipole cross-correlation between the C^i CSA and the C^jH^k dipolar interaction $\{i,j =$ methyl, next$\}$ and $\{k = 1,2\}$. This is a *non-secular* interaction and leads to the creation of $I_+S_+ \rightarrow 2I_+S_+H_z^k$ and $I_-S_- \rightarrow 2I_-S_-H_z^k$. This interaction is averaged out by proton inversion or decoupling (as in the pulse sequence shown in Fig. 1).

(v) CSA–CSA cross-correlation between the CSAs of C^i and C^j $\{i,j =$ methyl, next; $i \neq j\}$. This is a *secular* interaction and is not averaged out in the pulse sequence of Fig. 1.

(vi) Cross-correlation between the isotropic chemical shifts of C^i and C^j $\{i,j =$ methyl, next; $i \neq j\}$ due to chemical exchange. This is a *secular* interaction and not averaged out in the pulse sequence of Fig. 1.

Thus, the *secular* interactions represented by (i), (v), and (vi) appear in Eq. (5) (the C^i–C^j cross-relaxation is also secular and appears in Eq. (5)), while the *non-secular* interactions, (ii) and (iii) lead to multi-exponential relaxation of the DQC/ZQC at long mixing times. The *non-secular* interaction (iv) is averaged out by the pulse sequence shown in Fig. 1.

The evolution of the spin-system may be best studied in the subspace spanned by the four individual lines (doublet of doublets) of the $IS\mathrm{H}^1\mathrm{H}^2$ (AMXX′) system represented by the four single transition operators $B_{\mathrm{DQ}} = \{2I_+S_+H_\alpha^1H_\alpha^2, 2I_+S_+H_\alpha^1H_\beta^2, 2I_+S_+H_\beta^1H_\alpha^2, 2I_+S_+H_\beta^1H_\beta^2\}$ in the DQ manifold with corresponding operators in the ZQ manifold. Note, that formally, when one of the protons is a methyl proton in a fully protonated system, one needs to consider an $AMXX'_3$ system. However, the simplified treatment provided here should suffice in the present context. Let us first consider the case where both H^1 and H^2 are local protons with $J_{IH^1} = J_{SH^2} = {}^1J_{\mathrm{CH}}$ and $J_{IH^2} = J_{SH^1} = {}^2J_{\mathrm{CH}} \approx 0$. Evolution, the DQ manifold is given by [5]

$$\frac{\mathrm{d}B_{++}}{\mathrm{d}t} = -\Gamma_{++}B_{++} \tag{A.1}$$

and the Liouvillian Γ_{++} is represented by

$$\Gamma_{++} = \begin{pmatrix} \mathrm{i}\pi J_{++} + R_{DQ\alpha\alpha} + R_{av} & \frac{R_{ii}+R_{ai}-R_{ia}-R_{aa}}{4} & \frac{R_{ii}-R_{ai}+R_{ia}-R_{aa}}{4} & \frac{R_{ii}-R_{ai}-R_{ia}+R_{aa}}{4} \\ \frac{R_{ii}+R_{ai}-R_{ia}-R_{aa}}{4} & \mathrm{i}\pi J_{+-} + R_{DQ\alpha\beta} + R_{av} & \frac{R_{ii}-R_{ai}-R_{ia}+R_{aa}}{4} & \frac{R_{ii}-R_{ai}+R_{ia}-R_{aa}}{4} \\ \frac{R_{ii}-R_{ai}+R_{ia}-R_{aa}}{4} & \frac{R_{ii}-R_{ai}-R_{ia}+R_{aa}}{4} & -\mathrm{i}\pi J_{+-} + R_{DQ\beta\alpha} + R_{av} & \frac{R_{ii}+R_{ai}-R_{ia}-R_{aa}}{4} \\ \frac{R_{ii}-R_{ai}-R_{ia}+R_{aa}}{4} & \frac{R_{ii}-R_{ai}+R_{ia}-R_{aa}}{4} & \frac{R_{ii}+R_{ai}-R_{ia}-R_{aa}}{4} & -\mathrm{i}\pi J_{++} + R_{DQ\beta\beta} + R_{av} \end{pmatrix} \tag{A.2}$$

$R_{\mathrm{DQ}_{ij}}$ $i,j = \alpha,\beta$ are the autorelaxation rates of the four lines of the DQ spectrum. R_{ii}, R_{ia}, R_{ai}, and R_{aa} are the relaxation rates of the $2I_xS_x$, $4I_xS_xH_z^1$, $4I_xS_xH_z^2$ and $8I_xS_xH_z^1H_z^2$ coherences, respectively; $R_{av} = \frac{R_{ii}+R_{ia}+R_{ai}+R_{aa}}{4}$ and $J_{++} \approx 2^1J_{\mathrm{CH}}$. However, $J_{+-} \approx 0$ making the central two lines overlap *violating the secular approximation.* However, the off-diagonal elements under consideration in Eq. A.2

$$\begin{aligned}(\Gamma_{++})_{2,3} = (\Gamma_{++})_{3,2} &= \frac{R_{ii} - R_{ia} - R_{ai} + R_{aa}}{4} \\ &\approx \frac{R_{ii} - (R_{ii} + R_{1,\mathrm{H}}) - (R_{ii} + R_{1,\mathrm{H}}) + (R_{ii} + 2R_{1,\mathrm{H}})}{4} \\ &\approx 0\end{aligned} \tag{A.3}$$

$R_{1,\mathrm{H}}$ is the proton homonuclear spin–lattice relaxation. The off-diagonal elements $(\Gamma_{++})_{i,j} = (\Gamma_{++})_{j,i}$ $\{ij = 12, 14, 13, 24, 34\}$ may also be neglected if the following condition holds $8\pi^1J_{\mathrm{CH}} \gg |R_{1,H}|$, which is true for small and medium-sized proteins. Thus the decay of the DQC may be considered to be mono-exponential with the relevant rate (Γ_{DQ}) given by the sum of the diagonal elements of the dissipative part of Γ_{++} in Eq. (A.2).

However, for interactions involving remote protons, with no resolved scalar couplings to either the I or the S spins, both J_{++} and J_{+-} are zero and all four lines of the DQ spectrum overlap, *violating the secular approximation.* For the two central lines, the same arguments as above can be invoked. However for the outer lines, the magnitude of the largest of the relevant diagonal elements is $\frac{R_{1,\mathrm{H}}}{2}$ and this leads to multi-exponential decay at long mixing times. Similar analyses apply for the ZQ manifold. Fortunately, as pointed out in the text, remote dipolar interactions do not play a major role in the relaxation of DQC and ZQC. However, care has to be taken in analyzing the relaxation of DQC and ZQC at very long mixing times.

Appendix B. Relative sensitivities of auto- and cross-correlated order parameters involving methyl groups

It is of interest to investigate the relative sensitivities of the quantity $S^2_{\mathrm{cross,eff}} = [3S^2_{\mathrm{axis}}P_2(\cos 2\theta_{nm})P_2(\cos 2\theta_{mm}) + nS^2_{k,\mathrm{cross}}]$ (assuming $S^2_{\mathrm{axis}} = 1$) which may be considered an effective dipole–dipole cross-correlated order-parameter (“effective”, since it involves two different cross-correlation effects—(i) and (ii) as discussed in the text) with an auto-correlated order-parameter for the $C^{\mathrm{next}}H^{\mathrm{next}}$ dipolar interaction ($S^2_{\mathrm{next,auto}}$), with the degree of motion about the $C^{\mathrm{next}}C^{\mathrm{methyl}}$ axis, i.e., with γ. We have assumed that the only motion involved is the single-axis diffusion motion

of H^{next} and there is no anisotropic motion that affects the $C^{next}H^{methyl}$ and $C^{next}H^{next}$ dipolar interactions differently. Analysis of Fig. B1 reveals that $S^2_{next,auto}$ shows a rapid decline with increasing mobility until a value of approximately 90° is reached for γ and 0.25 for $S^2_{next,auto}$ (followed by a slower decline to its limiting value of 0.11 for $\gamma = 180°$). $S^2_{cross,eff}$ however, continues to be sensitive to motion for the full range of γ. It is evident that $S^2_{next,auto}$ is more sensitive to dynamics for smaller values of γ, i.e., less motion. Further, $S^2_{next,auto}$ and $S^2_{cross,eff}$ seem to correlate almost linearly until a value of approximately -0.7 for $S^2_{cross,eff}$ (corresponding to a γ value of approximately 90°—Fig. B2) followed by a significant deviation from linearity (when the $S^2_{next,auto}$ becomes relatively less responsive to motion). Thus, auto-correlated relaxation measurements involving the measurement of the dipolar relaxation of the $C^{next}H^{next}$ bond vectors would be less efficient in distinguishing between moderate amount of motion ($\gamma \approx 90°$) and complete disorder ($\gamma \approx 180°$) than the corresponding measurements of $S^2_{cross,eff}$. Thus even in the absence of anisotropic motion simple geometric considerations make

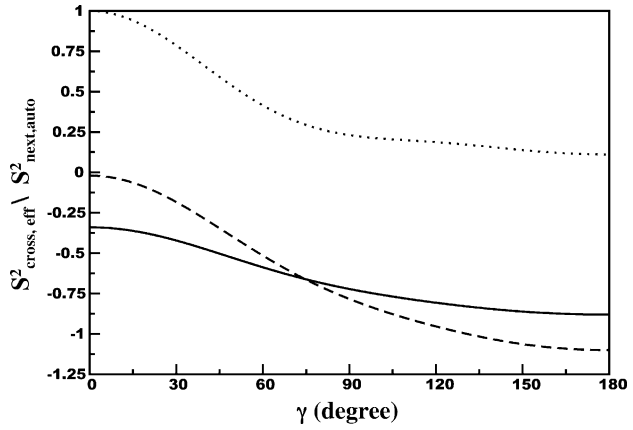

Fig. B1. Plots of $S^2_{next,auto}$ (dotted line), $S^2_{cross,eff}$ for all coherences except Ile, $C^{\gamma 1}$–$C^{\delta 1}$ (solid line) and $S^2_{cross,eff}$ for Ile $C^{\gamma 1}$–$C^{\delta 1}$ coherences (dashed line).

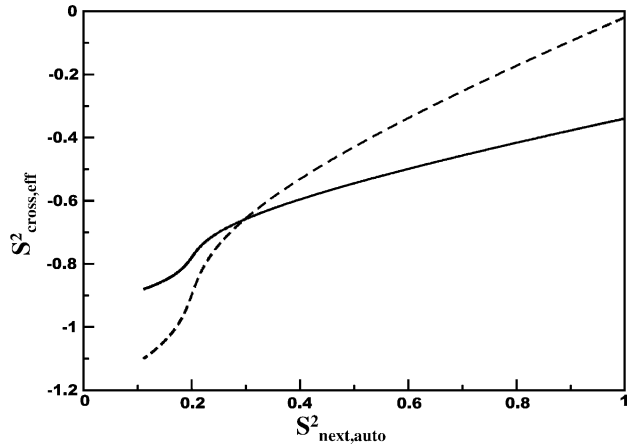

Fig. B2. Correlation between $S^2_{cross,eff}$ for all coherences except Ile, $C^{\gamma 1}$–$C^{\delta 1}$ (solid line) and for $C^{\gamma 1}$–$C^{\delta 1}$ coherences (dashed line) against $S^2_{next,auto}$.

the sensitivities of different measurements of the same motion be different depending on the extent of the motion being probed.

Appendix C. Effect of more complicated motional models on $\Delta\Gamma^{dd}_{local}/S^2_{axis}$ values

It has been mentioned in the main text that the simple single axis diffusion model (Model 1) is inappropriate for several residues in the protein core. Some other models that may be considered while analyzing the relaxation rates are discussed below.

C.1. Model 2—correlated motion about multiple axes

Let us consider, for example, the Ile $C^{\beta}H^{\beta}$ bond and assume that it undergoes restricted rotation about both the $C^{\beta}C^{\gamma 2}$ as well as the $C^{\beta}C^{\gamma 1}$ axes. This may be considered to be the diffusive motion of the point of intersection between the $C^{next}H^{k}$ and $C^{methyl}H^{k}$ dipolar vectors on the surface of a sphere rather than in a circular orbit as shown in Fig. 5c in the main text. $\Delta\Gamma^{dd}_{local}/S^2_{axis}$ in this case can be calculated using expressions provided by Daragan and Mayo [47]

$$\frac{\Delta\Gamma^{dd}_{local}}{S^2_{axis}} = 2\left(\frac{2}{5}\tau_C\right)\left(\frac{\mu_0\hbar}{4\pi}\right)^2\frac{\gamma_H^2\gamma_C^2}{r_1^3 r_2^3}[0.32 - 0.70(\Delta\gamma_1)^2 - 0.89(\Delta\gamma_2)^2 + 0.84c_{12}\Delta\gamma_1\Delta\gamma_2 - 0.66], \quad (C.1)$$

where $\Delta\gamma_1$ and $\Delta\gamma_2$ represent the root mean square deviation about each axis and c_{12} represents the correlation coeffficient for the two motional modes. For perfect correlation for the diffusion about the two axes, $c_{12} = 1$ and for perfect anti-correlation, $c_{12} = -1$. If the two motional modes are independent of each other then, $c_{12} = 0$. The variation of $\Delta\Gamma^{dd}_{local}/S^2_{axis}$ with $\Delta\gamma_1$ and $\Delta\gamma_2$ is plotted in Fig. C1.

C.2. Model 3—jumps between three non-equivalent sites

It has been noted that for buried sidechains, a valid motional model consists of jumps between three conformational states denoted by $\chi_1 = -60°$ (*gauche*−), $\chi_1 = 180°$ (anti) and $\chi_1 = +60°$ (*gauche*+) states. In the simplest of jump models, transitions between *gauche*+ and *gauche*− are disallowed and anti → *gauche*+ and anti → gauche− transitions occur with equal probability. In such a case, the $\Delta\Gamma^{dd}_{local}/S^2_{axis}$ may be written using expressions provided by London and Avitable [48] and Daragan and Mayo [36]

$$\frac{\Delta\Gamma^{dd}_{local}}{S^2_{axis}} = 2\left(\frac{2}{5}\tau_C\right)\left(\frac{\mu_0\hbar}{4\pi}\right)^2\frac{\gamma_H^2\gamma_C^2}{r_1^3 r_2^3} \times \left[-0.22 + 0.39\left\{P + (1-P)\cos\left(\frac{2\pi}{3}\right)\right\}^2 + 0.15\left\{P + (1-P)\cos\left(\frac{4\pi}{3}\right)\right\}^2 - 0.66\right], \quad (C.2)$$

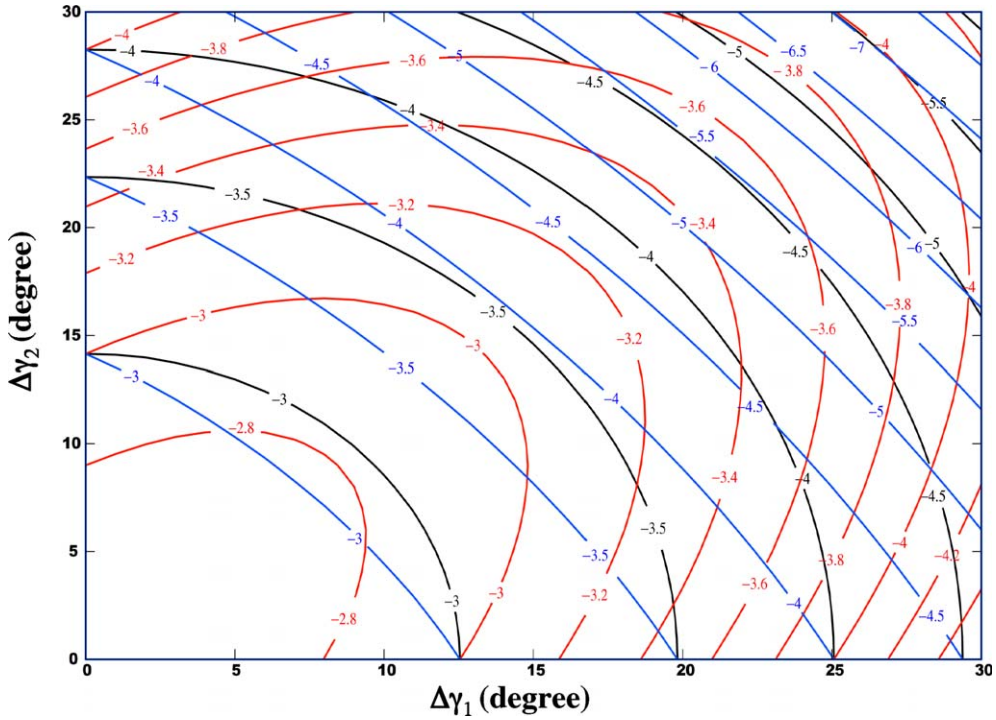

Fig. C1. Contour plots of $\Delta\Gamma^{dd}_{local}/S^2_{axis}$ against $\Delta\gamma_1$ and $\Delta\gamma_2$ values for uncorrelated ($c_{12}=0$, black), perfectly correlated ($c_{12}=1$, red) and perfectly anti-correlated ($c_{12}=-1$, blue) motion for the two-axis motion model (Model 2).

where P is the probability of finding the system in the anti position (or its fractional occupancy). The $\Delta\Gamma^{dd}_{local}/S^2_{axis}$ values are plotted against P in Fig. C2. The situation can be even more dramatic in the case where the anti $\rightarrow$ *gauche*+ and anti $\rightarrow$ *gauche*− do not occur with equal probability. This is a more likely scenario in real proteins, especially in buried sidechains, the asymmetric steric environment making the populations of the *gauche*+ or the *gauche*− unequal, see for example Chou et al. [40].

C.3. Model 4—conformational jumps coupled between three non-equivalent sites coupled with restricted diffusion about each site

Assuming the jump model described above and in addition allowing the χ_1 to deviate by an amount $\Delta\chi$ from its mean position (the deviation is assumed to be the same for the three sites and to occur on a timescale much faster than the conformational jumps) we obtain an expression for $\Delta\Gamma^{dd}_{local}/S^2_{axis}$ following Daragan and Mayo [36]

$$\frac{\Delta\Gamma^{dd}_{local}}{S^2_{axis}} = 2\left(\frac{2}{5}\tau_C\right)\left(\frac{\mu_0\hbar}{4\pi}\right)^2\frac{\gamma_H^2\gamma_C^2}{r_1^3r_2^3} \times\left[-0.22+0.39\left\{P+(1-P)\cos\left(\frac{2\pi}{3}\right)\right\}^2 +0.15\left\{P+(1-P)\cos\left(\frac{4\pi}{3}\right)\right\}^2-1.98(\Delta\gamma)^2-0.66\right]. \quad (C.3)$$

This model represents transitions within a triple well with equal widths about the three minima as opposed to zero well widths in model 3 described above. Again, the situation is much more complicated in real systems which are expected to involve transitions within a triple well with different widths about the three minima. The variation of $\Delta\Gamma^{dd}_{local}/S^2_{axis}$ with P and $\Delta\chi$ is shown in Fig. C3. Note that in calculating $\Delta\Gamma^{dd}_{local}/S^2_{axis}$ for all models discussed (1–4), unrestricted single axis diffusion of the methyl group has been assumed.

Recall that the estimated value of $\Delta\Gamma^{dd}_{local}/S^2_{axis}$ for unrestricted single-axis diffusive motion was calculated to be $-6.90\ s^{-1}$ ($\gamma=180°$, Model 1—see main text). A larger value absolute value ($-7.89\ s^{-1}$) is obtained for a much smaller degree of motion ($\Delta\gamma_1=30°$ and $\Delta\gamma_2=30°$) when the motions about each of the two axes are perfectly anti-correlated. The corresponding values for positively correlated and uncorrelated motion are -4.28 and $-6.08\ s^{-1}$. Thus, the presence of correlated multiple-axis diffusion (Model 2) produces results more consistent with that expected from the S^2_{axis} values (see main text). For a jump model (Model 3), a $\Delta\Gamma^{dd}_{local}/S^2_{axis}$ value of $-6.90\ s^{-1}$ is reproduced, for example, by a 27% occupancy of the anti-state. For a three-site jump model with additional motion about the three sites (Model 4) a $\Delta\Gamma^{dd}_{local}/S^2_{axis}$ value of $-6.90\ s^{-1}$ is reproduced, for example, by a 10% occupancy of the anti-site with an additional motional amplitude of 15° about the *gauche*+/− and anti-sites. *Thus, the need to invoke larger amounts of motion to obtain a particular* $\Delta\Gamma^{dd}_{local}/S^2_{axis}$ *value decreases as the motional model becomes*

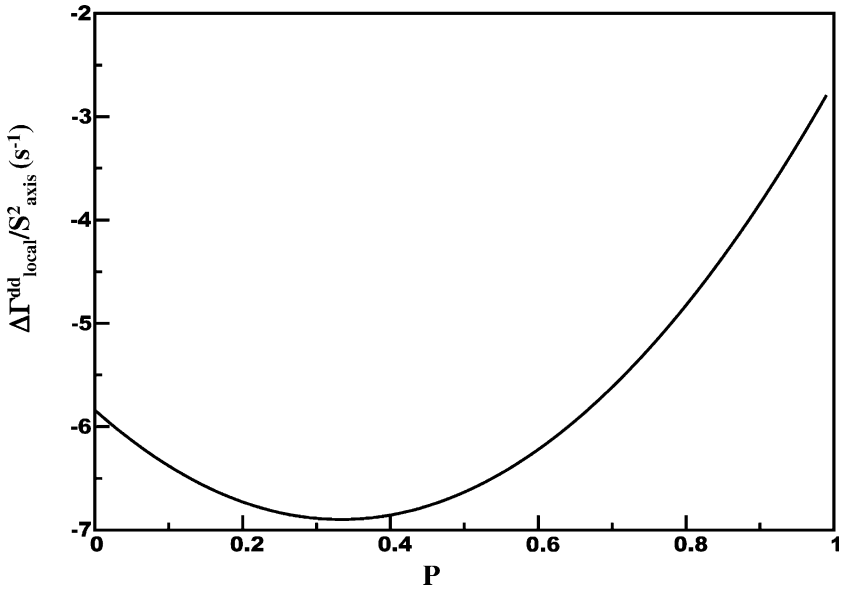

Fig. C2. Plot of $\Delta\Gamma^{dd}_{local}/S^2_{axis}$ against P, the occupancy of the anti site for the three-site jump model (Model 3).

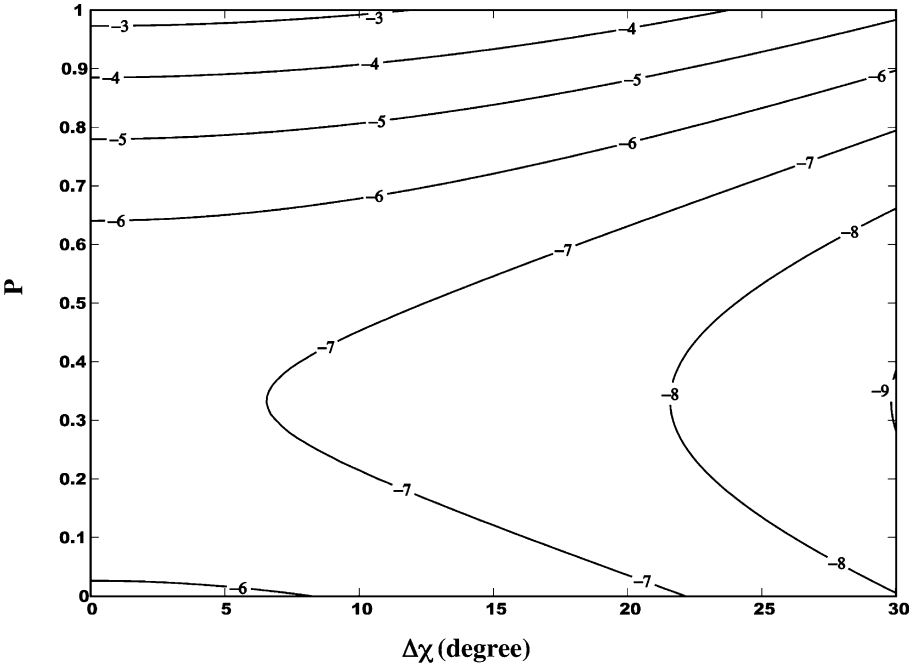

Fig. C3. Contour plot of the variation of $\Delta\Gamma^{dd}_{local}/S^2_{axis}$ with P and $\Delta\chi$ values for the three-site jump with additional restricted diffusion (Model 4).

more complex. The appropriateness of a motional model cannot be determined in the absence of other measurements or molecular dynamics simulations.

References

[1] A. Kumar, R.C.R. Grace, P.K. Madhu, Cross-correlations in NMR, Prog. Nucl. Magn. Reson. Spectrosc. 37 (2000) 191–319.

[2] D. Frueh, Internal motions in proteins and interference effects in nuclear magnetic resonance, Prog. Nucl. Magn. Reson. Spectrosc. 41 (2002) 305–324.

[3] M.W.F. Fischer, L. Zeng, Y. Pang, W. Hu, A. Majumdar, E.R.P. Zuiderweg, Experimental characterization of models for backbone picosecond dynamics in proteins. Quantification of NMR auto- and cross-correlation relaxation mechanisms involving different nuclei of the peptide plane, J. Am. Chem. Soc. 119 (1997) 12629–12642.

[4] B. Reif, M. Hennig, C. Griesinger, Direct measurement of angles between bond vectors in high-resolution NMR, Science 276 (1997) 1230–1233.

[5] E. Chiarparin, P. Pelupessy, R. Ghose, G. Bodenhausen, Relaxation of two-spin coherence due to cross-correlated fluctuations of dipole–dipole couplings and anisotropic shifts in NMR of ^{15}N, ^{13}C-labeled biomolecules, J. Am. Chem. Soc. 121 (1999) 6876–6883.

[6] E. Chiarparin, P. Pelupessy, R. Ghose, G. Bodenhausen, Relative orientation of C^{α} H^{α} bond vectors of successive residues in proteins through cross-correlated relaxation in NMR, J. Am. Chem. Soc. 122 (2000) 1758–1761.

[7] H. Schwalbe, T. Carlomagno, M. Hennig, J. Junker, B. Reif, C. Richter, C. Griesinger, Cross-correlated relaxation for measurement

of angles between tensorial interactions, Methods Enzymol. 338 (2001) 35–81.
[8] D. Fushman, N. Tjandra, D. Cowburn, Direct measurement of ^{15}N chemical shift anisotropy in solution, J. Am. Chem. Soc. 120 (1998) 10947–10952.
[9] D. Fushman, D. Cowburn, Model-independent analysis of ^{15}N chemical shift anisotropy from NMR relaxation data. Ubiquitin as a test example, J. Am. Chem. Soc. 120 (1998) 7109–7110.
[10] C.D. Kroenke, M. Rance, A.G. Palmer III, Variability of the ^{15}N chemical shift anisotropy in Escherichia coli ribonuclease H in solution, J. Am. Chem. Soc. 121 (1999) 10119–10125.
[11] K. Loth, P. Pelupessy, G. Bodenhausen, Chemical shift anisotropy tensors of carbonyl, nitrogen, and amide proton nuclei in proteins through cross-correlated relaxation in NMR spectroscopy, J. Am. Chem. Soc. 127 (2005) 6062–6068.
[12] N. Tjandra, A. Bax, Large variations in ^{13}C chemical shift anisotropy in proteins correlate with secondary structure, J. Am. Chem. Soc. 119 (1998) 9566–9567.
[13] Y. Pang, E.R.P. Zuiderweg, Determination of protein backbone ^{13}CO chemical shift anisotropy tensors in solution, J. Am. Chem. Soc. 122 (2000) 4841–4842.
[14] F. Cisnetti, K. Loth, P. Pelupessy, G. Bodenhausen, Determination of chemical shift anisotropy tensors of carbonyl nuclei in proteins through cross-correlated relaxation in NMR, ChemPhysChem 5 (2004) 807–814.
[15] B. Brutscher, Principles and applications of cross-correlated relaxation in biomolecules, Concepts Magn. Reson. 12 (2000) 207–229.
[16] K. Kloiber, R. Konrat, Differential multiple-quantum relaxation arising from cross-correlated time-modulation of isotropic chemical shifts, J. Biomol. NMR 18 (2000) 33–42.
[17] D. Frueh, J.R. Tolman, G. Bodenhausen, C. Zwahlen, Cross-correlated chemical shift modulation: a signature of slow internal motions proteins, J. Am. Chem. Soc. 123 (2001) 4810–4816.
[18] R. Bruschweiler, R.R. Ernst, Molecular dynamics monitored by cross-correlated cross relaxation of spins quantized along orthogonal axes, J. Chem. Phys. 96 (1992) 1758–1766.
[19] J. Wist, D. Frueh, J.R. Tolman, G. Bodenhausen, Triple quantum decoherence under multiple refocusing: Slow correlated chemical shift modulations of C' and N nuclei in proteins, J. Biomol. NMR 28 (2004) 263–272.
[20] D.M. Korzhnev, K. Kloiber, L.E. Kay, Multiple-quantum relaxation dispersion NMR spectroscopy probing millisecond time-scale dynamics in proteins: Theory and application, J. Am. Chem. Soc. 126 (2004) 7320–7329.
[21] A. Majumdar, R. Ghose, Probing slow backbone dynamics in proteins using TROSY-based experiments to detect cross-correlated time-modulation of isotropic chemical shifts, J. Biomol. NMR 28 (2004) 213–227.
[22] A.G. Palmer III, C.D. Kroenke, J.P. Loria, Nuclear magnetic resonance methods for quantifying microsecond-to-millisecond motions in biological macromolecules, Methods Enzymol. 339 (2001) 204–238.
[23] L. Vugmeyster, C. Perazzolo, J. Wist, D. Frueh, G. Bodenhausen, Evidence of slow motions by cross-correlated chemical shift modulation in deuterated and protonated proteins, J. Biomol. NMR 28 (2004) 173–177.
[24] V. Tugarinov, P.M. Hwang, J.E. Ollerenshaw, L.E. Kay, Cross-correlated relaxation enhanced ^{1}H-^{13}C NMR spectroscopy of methyl groups in very high molecular weight proteins and protein complexes, J. Am. Chem. Soc. 125 (2003) 5701–5706.
[25] D.M. Korzhnev, K. Kloiber, V. Kanelis, V. Tugarinov, L.E. Kay, Probing slow dynamics in high molecular weight proteins by methyl-TROSY NMR spectroscopy: application to a 723-residue enzyme, J. Am. Chem. Soc. 126 (2004) 3964–3973.
[26] A.L. Lee, P.F. Flynn, A.J. Wand, Comparison of ^{2}H and ^{13}C NMR relaxation techniques for the study of protein methyl group dynamics in solution, J. Am. Chem. Soc. 121 (1999) 2891–2902.
[27] D. Yang, A. Mittermaier, Y.K. Mok, L.E. Kay, A study of protein side-chain dynamics from new ^{2}H auto-correlation and ^{13}C cross-correlation NMR experiments: application to the N-terminal SH3 domain from drk, J. Mol. Biol. 276 (1998) 939–954.
[28] M. Goldman, Quantum Description of High-Resolution NMR in Liquids, Oxford University Press, New York, 1991.
[29] J. Dittmer, G. Bodenhausen, Evidence for slow motion in proteins by multiple refocusing of heteronuclear nitrogen/proton multiple quantum coherences in NMR, J. Am. Chem. Soc. 126 (2004) 1314–1315.
[30] A.G. Palmer, J. Cavanagh, P.E. Wright, M. Rance, Sensitivity improvement in proton-detected 2-dimensional heteronuclear correlation NMR-spectroscopy, J. Magn. Reson. 93 (1991) 151–170.
[31] R. Ghose, J.H. Prestegard, Improved estimation of CSA-dipolar coupling cross-correlation rates from laboratory-frame relaxation experiments, J. Magn. Reson. 134 (1998) 308–314.
[32] F. Delaglio, S. Grzesiek, G.W. Vuister, G. Zhu, J. Pfeifer, A. Bax, NMRPipe: a multidimensional spectral processing system based on UNIX pipes, J. Biomol. NMR 6 (1995) 277–293.
[33] P.T. Boggs, J.R. Donaldson, R.H. Byrd, R.B. Schnabel, ODRPACK software for weighted orthogonal distance regression, ACM Trans. Math. Software 15 (1989) 348–364.
[34] B.J. Wylie, W.T. Franks, D.T. Graesser, C.M. Reinstra, Site-specific ^{13}C chemical shift anisotropy measurements in a uniformly ^{15}N,^{13}C-labeled microcrystalline protein by 3D magic-angle spinning NMR spectroscopy, J. Am. Chem. Soc. 127 (2005) 11946–11947.
[35] A.L. Lee, A.J. Wand, Assessing potential bias in the determination of rotational correlation times of proteins by NMR relaxation, J. Biomol. NMR 13 (1999) 101–112.
[36] V.A. Daragan, K.H. Mayo, Motional model analyses of protein and peptide dynamics using ^{13}C and ^{15}N NMR relaxation, Prog. Nucl. Magn. Reson. Spectrosc. 31 (1997) 63–105.
[37] G.M. Clore, A. Szabo, A. Bax, L.E. Kay, P.C. Driscoll, A.M. Gronenborn, Deviations from the simple two-parameter model-free approach to the interpretation of nitrogen-15 nuclear magnetic relaxation of proteins, J. Am. Chem. Soc 112 (1990) 4936–4989.
[38] P. Kumar, A. Kumar, Effect of dipolar cross-correlations on the transverse relaxation of single- and multiple-quantum coherences in strongly coupled spin systems, J. Magn. Reson. A 115 (1995) 155–164.
[39] R.B. Best, J. Clarke, M. Karplus, What contributions to protein side-chain dynamics are probed by NMR experiments?. A molecular dynamics simulation analysis, J. Mol. Biol. 349 (2005) 185–203.
[40] J.J. Chou, D.A. Case, A. Bax, Insights into the mobility of methyl-bearing side chains in proteins from $^{3}J_{CC}$ and $^{3}J_{CN}$ couplings, J. Am. Chem. Soc. 125 (2003) 8959–8966.
[41] K. Lindorff-Larsen, R.B. Best, M.A. Depristo, C.M. Dobson, M. Vendruscolo, Simultaneous determination of protein structure and dynamics, Nature 433 (2005) 128–132.
[42] A.J. Wand, J.L. Urbauer, R.P. McEvoy, R.J. Bieber, Internal dynamics of human ubiquitin revealed by ^{13}C-relaxation studies of randomly fractionally labeled protein, Biochemistry 35 (1996) 6116–6125.
[43] V.Y. Orekhov, D.M. Korzhnev, L.E. Kay, Double- and zero-quantum NMR relaxation dispersion experiments sampling millisecond time scale dynamics in proteins, J. Am. Chem. Soc. 126 (2004) 1886–1891.
[44] E. Oldfield, Chemical shifts in amino acids, peptides, and proteins: from quantum chemistry to drug design, Annu. Rev. Phys. Chem. 53 (2002) 349–378.
[45] T. Lazaridis, M. Karplus, Effective energy function for proteins in solution, Proteins 35 (1999) 133–152.
[46] H. Geen, R. Freeman, Band-selective radiofrequency pulses, J. Magn. Reson. 93 (1991) 93–141.
[47] V. Daragan, K.H. Mayo, Analysis of internally restricted correlated rotations in peptides and proteins using ^{13}C and ^{15}N relaxation data, J. Phys. Chem. 100 (1996) 8378–8388.
[48] R.E. London, J. Avitable, Calculation of carbon-13 relaxation times and nuclear Overhauser enhancements in a hydrocarbon chain undergoing gauche-trans isomerism, J. Am. Chem. Soc. 99 (1977) 7765–7776.